[American Journal of Science, Vol. 311, November, 2011, P. 773–812, DOI 10.2475/09.2011.02]

THREE Fe-Ti OXIDE ORE-BEARING GABBRO-GRANITOID COMPLEXES IN THE PANXI REGION OF THE PERMIAN EMEISHAN LARGE IGNEOUS PROVINCE, SW CHINA

J. GREGORY SHELLNUTT*,†, KUO-LUNG WANG**, GEORG F. ZELLMER**, YOSHIYUKI IIZUKA**, BOR-MING JAHN***, KWAN-NANG PANG***, LIANG QI§, and MEI-FU ZHOU§§

ABSTRACT. The Permian (~260 Ma) Emeishan large igneous province of SW China contains three nearly identical gabbro-granitoid complexes that host giant Fe-Ti oxide deposits. The Fe-Ti oxide deposits are within the lower portions of evolved layered gabbroic intrusions and are spatially and temporally associated with A-type granitic plutons. The 264 ± 3 Ma Taihe layered gabbroic intrusion hosts a large magmatic Fe-Ti oxide deposit and is coeval with the Taihe peralkaline, A-type granitic pluton, which is dated at 261 ± 2 Ma. Within the A-type granitic pluton are microgranular enclaves, which have compositions intermediate between the gabbro and host granite. Primitive mantle-normalized incompatible element plots show corresponding reciprocal patterns between the mafic and felsic rocks. The chondrite-normalized REE patterns show Eu-anomalies changing from positive (Eu/Eu* = 1.5 to 5.9) in the gabbroic intrusion to negative in the enclaves (Eu/Eu* = 0.4 to 0.6) and granites (Eu/Eu* = 0.2 to 0.5). Whole rock $\varepsilon Nd_{(T)}$ values of the gabbroic intrusion ($\varepsilon Nd_{(T)}$ = +2.5 to +3.3) are similar to those of the enclaves ($\varepsilon Nd_{(T)}$ = +1.0 to 2.0) and granite ($\varepsilon Nd_{(T)}$ = +1.5 to +1.9) whereas the zircon $\varepsilon Hf_{(T)}$ values of the gabbro ($\varepsilon Hf_{(T)}$ = +8.1 ± 0.8) are indistinguishable from those of the granites ($\varepsilon Hf_{(T)}$ = +9.2 ± 1.0), suggesting that the parent magmas for all rock types originated from the same mantle source. Geochemical modeling indicates that the gabbros and granites can be generated by fractional crystallization of a common parental magma similar to high-Ti Emeishan flood basalt. The compositional jump from the gabbro to the enclaves is attributed to the crystallization of Fe-Ti oxide minerals. The results of this study and other studies suggest that the magmatic conditions (for example, pressure, composition, fO_2), which led to the formation of at least three Fe-Ti oxide bearing gabbro-granitoid complexes, were relatively common during the development of the Emeishan large igneous province.

Key words: Late Permian, Fe-Ti oxide deposit, layered gabbro, Emeishan large igneous province, fractional crystallization, A-type granites

INTRODUCTION

The petrogenesis of layered mafic-ultramafic intrusions continues to be a relevant and controversial topic in modern igneous petrological studies (Wager and Brown, 1968; Morse, 1996; Cawthorn, 1996; Veksler and others, 2007; Namur and others, 2011). These bodies are important for understanding the petrological development of magmas within the crust. Moreover, some layered intrusions contain economic concentrations of Ni, Cu, Fe, Ti, V and platinum-group elements (PGE) making them important targets for mineral exploration (McCallum, 1996; Eales and Cawthorn, 1996; Lee, 1996; Maier and others, 2003; Zhou and others, 2008). Spatially and temporally associated with many layered ultramafic-mafic intrusions are granitic

* National Taiwan Normal University, Department of Earth Sciences, 88 Tingzhou Road Section 4, Taipei 11677, Taiwan
** Academia Sinica, Institute of Earth Sciences, 128 Academia Road Section 2, Nankang Taipei 11529, Taiwan
*** National Taiwan University, Department of Geosciences, P.O. Box 13-318, Taipei 10699, Taiwan
§ State Key Lab of Ore Deposit Geochemistry, Institute of Geochemistry, Chinese Academy of Sciences, Guiyang 550002, China
§§ Department of Earth Sciences, The University of Hong Kong, Pokfulam Road, Hong Kong SAR
† Corresponding author: E-mail: jgshelln@ntnu.edu.tw

plutons, which have chemical characteristics of "within-plate" or "A-type" granitoids (Weibe, 1996; Bonin, 2007). The relationship between the spatially associated, contemporaneous mafic-ultramafic intrusions and granitic plutons has been interpreted as evidence for silicate liquid immiscibility, fractional crystallization, crustal melting and separate magma suites (Huppert and Sparks, 1988; Ferreira and others, 1994; Morse, 1996; Weibe, 1996; Jakobson and others, 2005; Zhou and others, 2005; Veksler and others, 2006; Namur and others, 2011).

Large igneous provinces (LIP) are sites of spatially contiguous, rapidly emplaced magmatic rocks (mostly flood basalts), which represent regions of heat and mass transfer from the mantle to the crust (Bryan and Ernst, 2008). Exposed within some continental LIPs are felsic and mafic plutonic and hypabyssal rocks. Although their volumes are minor compared to the flood basalts, the plutonic rocks of LIPs often contain substantial mineral deposits (Schissel and Smail, 2001; Zhou and others, 2008). Within the Permian (~260 Ma) Emeishan large igneous province (ELIP) of SW China, there are at least five mafic to ultramafic intrusions which contain world-class Fe-Ti-V oxide deposits (Pang and others, 2010). Three of the intrusions are gabbroic and spatially associated with peralkaline, silica-saturated granitoids (Panzhihua, Baima, Taihe), whereas the other two are ultramafic in composition and are not necessarily associated with peralkaline granitoids (Hongge, Xinjie). Previous studies have indicated that the ultramafic intrusions formed by fractionation of primitive magmas, which assimilated crustal material, whereas the gabbroic intrusions and their associated granitic rocks formed by fractional crystallization of a common parental magma with minimal crustal assimilation (Zhong and others, 2002, 2004; Shellnutt and others, 2009a; Zhang and others, 2009; Shellnutt and Jahn, 2010; Tao and others, 2010). Unlike the Panzhihua and Baima gabbro-granitoid complexes, few studies have focused on the formation of the Taihe layered gabbroic intrusion. The petrogenetic relationship between the spatially associated Taihe peralkaline A-type pluton and the gabbro is contentious. It has been suggested that the Taihe peralkaline pluton is derived by crustal melting or is cogenetic but not comagmatic with the gabbro or that it was formed together with the layered gabbro by fractional crystallization of a common parental magma (Shellnutt and Zhou, 2007; Xu and others, 2008; Zhong and others, 2011).

In this paper, we present new whole-rock geochemical data, mineral chemistry and zircon U-Pb radiometric dating and Hf isotopic data for gabbroic rocks of the Fe-Ti-oxide bearing Taihe layered intrusion. We compare the results with other Fe-Ti-oxide bearing gabbro-granitoid complexes of the ELIP and evaluate whether the neighboring peralkaline, silica-saturated granite is related to the formation of the ore-bearing gabbros.

GEOLOGICAL SETTING

The Emeishan large igneous province (ELIP) covers an area of $\sim 0.3 \times 10^6$ km^2 within southwestern China and northern Vietnam and consists of flood basalts, felsic plutons and layered mafic-ultramafic intrusions with some of them hosting giant Fe-Ti-V oxide deposits or Ni-Cu sulphide deposits (fig. 1; Chung and Jahn, 1995; Ali and others, 2005; Wang and others, 2007; Zhou and others, 2008). The ELIP is located near the western edge of the Proterozoic Yangtze Block, at the boundary with the Early Triassic Songpan-Ganze terrane, and was dismembered during the Mesozoic and Cenozoic by post-emplacement faulting associated with the collision between the North China Block and South China Block and the Indo-Eurasian collision (Chung and Jahn, 1995; Liu and others, 2006). The volcanic succession includes picrites, basaltic andesites, rhyolites, trachytes and basalts, which are subdivided on the basis of TiO_2 weight percent and Ti/Y into high- and low-Ti groups. The high- and low-Ti basalts are considered by some to have separate origins, although this is subject to

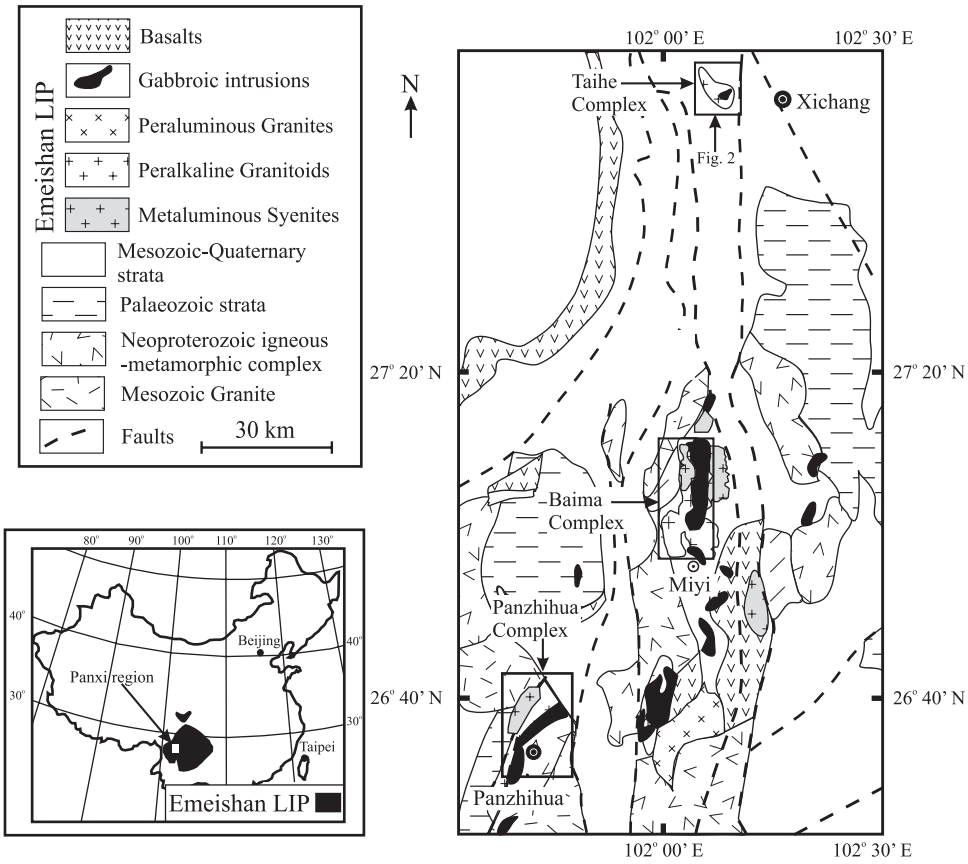

Fig. 1. Simplified geological map of the Panxi region showing the distribution of the Late Permian gabbro-granitoid complexes of the Emeishan large igneous province.

debate (Xu and others, 2001; Xiao and others, 2004; Wang and others, 2007; Fan and others, 2008; Hou and others, 2011; Shellnutt and Jahn, 2011). The basalt formations range in thickness from 1.0 to 5.0 km in the western part and 0.2 to 2.6 km in the eastern part of the ELIP. A mantle-plume is believed to be the cause of the geological features of the ELIP, such as the extensive flood basalts, ultramafic lavas, short eruptive duration (≤3 Ma), structural doming and lower crustal seismic velocity layers (Zhou and others, 2002; Xu and others, 2004; Ali and others, 2005; He and others, 2007). Furthermore, it is suggested that the emplacement of the Emeishan mafic magmas into carbonate rocks may have contributed to the decline of biota during the end-Guadaloupian mass extinction (Ganino and Arndt, 2009). Emeishan LIP volcanism was likely short lived, but it is possible that underplated mafic rocks may have served as a source for mafic and felsic magmas for an additional 20 million years or so (Xu and others, 2008; Shellnutt and others, 2008, 2011a).

The Panxi region, between the cities of Panzhihua and Xi Chang, of southern Sichuan province is an important area within the ELIP because plutonic and hypabyssal rocks are exposed including the Baima, Hongge, Panzhihua, Taihe and Xinjie mafic-ultramafic intrusions that host world-class orthomagmatic Fe-Ti-V oxide deposits. There are also numerous spatially and temporally associated granitic plutons, which range in composition from peraluminous to metaluminous to peralkaline

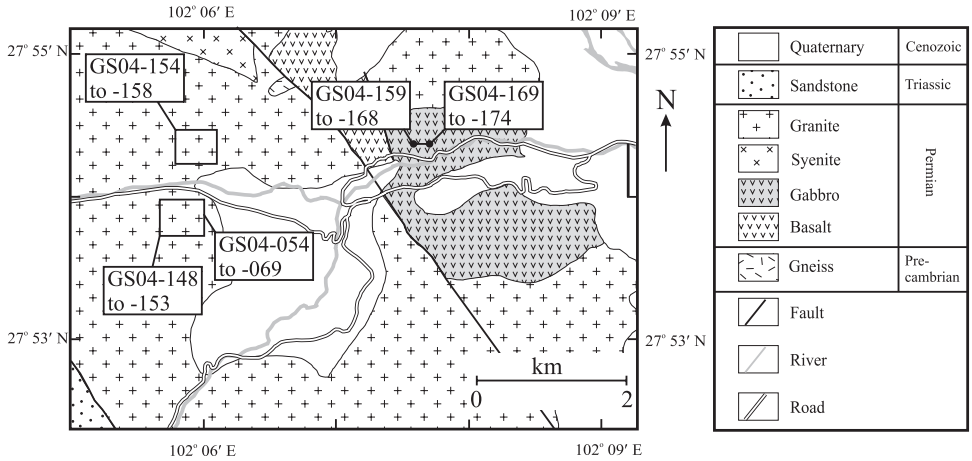

Fig. 2. Geological map of the Taihe gabbro-granite complex, showing the sampling localities (modified from Wang and others, 1993).

(Shellnutt and Zhou, 2007; Shellnutt and others, 2011b). The Panzhihua, Baima and Taihe gabbros are chemically evolved and spatially associated with peralkaline granitic rocks, whereas the Hongge and Xinjie intrusions are predominantly ultramafic (for example, pyroxenite) suggesting that there are petrogenetic differences between the two types of intrusions (Zhang and others, 2009; Tao and others, 2010).

The Taihe layered gabbroic intrusion is located to the west of the city of Xi Chang and is ovoid in shape (fig. 2). The intrusion has been described by Yao and others (1993) to consist of three silicate-rich zones and oxide-ores. The lower and middle gabbros consist of variable proportions of clinopyroxene (45-55 vol.%), plagioclase (15-25 vol.%), olivine (5-15 vol.%) and magnetite (10-15 vol.%). The middle gabbro zone contains the oxide ores which contain nearly 100 percent magnetite. The upper gabbro zone consists mostly of plagioclase (50-65 vol.%), clinopyroxene (20-25 vol.%), magnetite (5-10 vol.%) and apatite and hornblende (3-6 vol.%) (Zhong and others, 2011). Samples for geochemical analysis were collected at two sites within the Taihe open pit mine. The first group of samples (GS04-159 to −168) was collected from the central portion of the open pit, whereas the second group of samples (GS04-169 to −174) was collected ~100 meters to the east. Sample TH-1 was collected within the same area as the first group of samples. To the west of the gabbroic intrusion is the Taihe peralkaline granite, which is exposed in a series of quarries in the surrounding highland. The highland forms a catchment basin for a tributary of the An Ning River. The peralkaline granite is dated at 261 ± 2 Ma and is considered to be fault-bound with basalts and the gabbroic intrusion (Wang and others, 1993; Xu and others, 2008). The pluton contains several centimeter-sized mircogranular enclaves (Shellnutt and others, 2010).

PETROGRAPHY OF THE TAIHE ROCKS

The Taihe granites are coarse-grained and consist of perthitic alkali feldspar, quartz and amphibole with accessory titanite, aenigmatite, apatite, fluorite, ilmenite, Ce-monazite and aegirine. Alkali feldspar is euhedral to subhedral with fine, linear exsolution lamellae. The crystals are typically 1 to 2 cm in length and comprise ~65 to 70 volume percent of bulk mineralogy. Quartz is ≤0.2 cm in size and subhedral and interstitial to the feldspars, comprising 20 to 25 volume percent of the mode.

Amphiboles, predominantly ferrorichterite, are subhedral and interstitial to the feldspars and contain apatite inclusions. Some amphiboles are partially altered to reibeckite/arfvedsonite and have a translucent red-brown mineral. Small quantities (<1%) of subhedral aegirine, zircon, aenigmatite, Mn-rich ilmenite, apatite, Ce-monazite and fluorite are also present (Shellnutt and Iizuka, 2011).

The enclaves consist primarily of alkali feldspar, quartz and the sodic-calcic amphibole ferrorichterite. Alkali feldspar comprises ~70 volume percent of the mode and is typically medium- to fine-grained, euhedral to subhedral with perthitic exsolution lamellae. Although crystals are generally inclusion-free, a few larger crystals contain inclusions of amphibole. The amphiboles are fine- to medium-grained with subhedral to anhedral shapes and interstitial to the alkali feldspar. Quartz varies considerably in abundance from <5 volume percent to 20 volume percent of the mode and is medium- to fine-grained and interstitial to the alkali feldspars and amphiboles. The crystals are typically subhedral to anhedral. The only accessory mineral observed was apatite. In at least one case, there was a distinct texture of fine-grained, acicular amphibole within a very fine matrix of alkali feldspar.

The gabbros consist of coarse-grained cumulus olivine, plagioclase, clinopyroxene and interstitial oxide and sulphide minerals. Olivine is commonly equant with rounded edges and typically a few millimeters in size (≥2 mm). Some olivine is altered to serpentine. Plagioclase is typically euhedral to anhedral and ≤5 mm in size. Most crystals are tabular and have some saussuritic alteration. Rims of brown hornblende or biotite are common around the plagioclase when in contact with oxide minerals. Clinopyroxene crystals are similar in size and shape to the olivine crystals and have oxide exsolution lamellae (fig. 3A). Magnetite displays oxidation exsolution lamella of ilmenite and spinel (chromite and pleonaste) with minor amounts of sulphide mineral inclusions and is interstitial to the silicate minerals (figs. 3B and 3C). The mineral modes of the rocks are variable but generally olivine is ≤10 percent, plagioclase is between 45 percent and 55 percent, clinopyroxene is between 20 and 35 percent and oxide minerals are ≤10 percent in the silicate-rich samples. The Fe-Ti oxide ores contain ≤10 percent silicate minerals and ≥90 percent spinel minerals and ilmenite.

METHODS

Electron Microprobe Analysis

Mineralogical investigation of sample GS04-174 was carried out by a field emission electronprobe microanalyzer (FE-EPMA: JEOL JXA-8500F) equipped with five wavelength dispersive spectrometers (WDS) at the Institute of Earth Sciences, Academia Sinica in Taipei. Secondary- and back scattered electron images were used to guide the analysis on target positions of minerals. A 2 μm defocused beam was operated for quantitative analysis at an acceleration voltage of 12 kV with a beam current of 5nA. The measured X-ray intensities were corrected by the ZAF method using the standard calibration of synthetic chemical-known standard minerals with various diffracting crystals, as follows; wollastonite for Si with TAP crystal and Ca with PET crystal, rutile for Ti (PET), corundum for Al (TAP), chromium oxide for Cr (PET), fayalite for Fe with LiF crystal, tephroite for Mn (PET), pyrope for Mg (TAP), albite for Na (TAP), adularia for K (PET), apatite for P (PET), sodalite for Cl (PET) and fluorite for F (TAP). Peak counting times for the upper and lower baselines of each element were 10 sec and 5 sec, respectively.

Zircon U-Pb Geochronology

Zircon U-Pb isotopic analyses were preformed by laser ablation inductively coupled plasma mass spectrometry (LA-ICP-MS) at National Taiwan University in Taipei. The full set-up and methods are described by Chiu and others (2009). The laser ablation

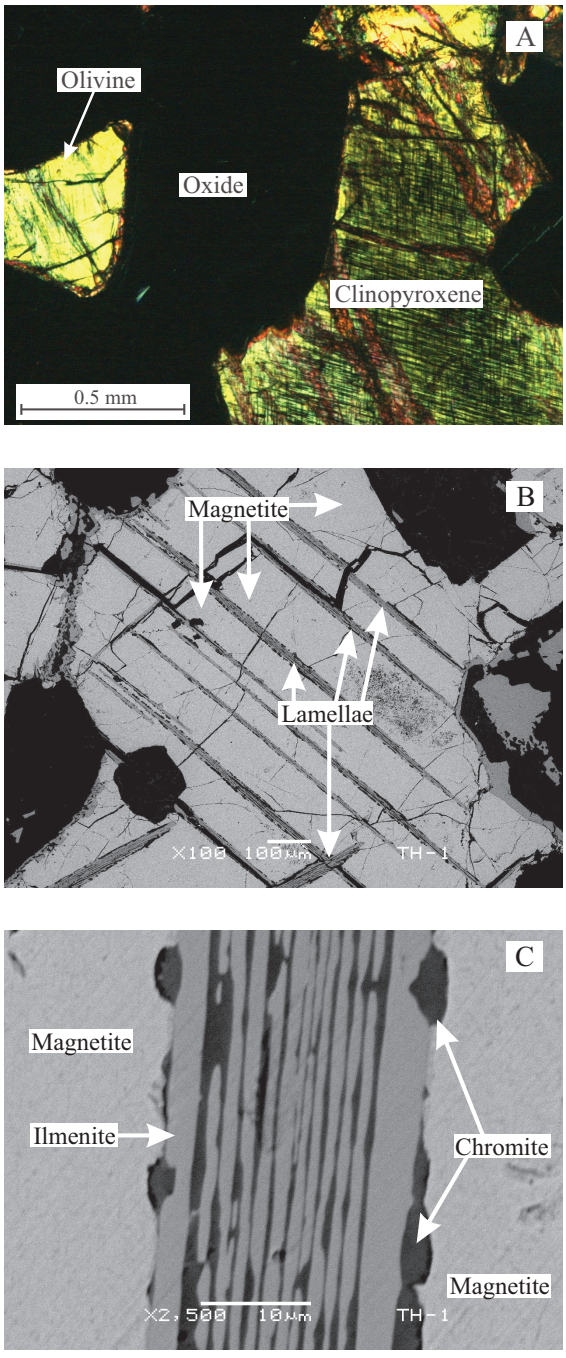

Fig. 3. (A) Photomicrograph of sample TH-1 showing olivine and clinopyroxene surrounded by oxide minerals. The thin black lines within the pyroxene are exsolution of oxides. (B) Back-scattered electron image of a magnetite crystal with oxidation exsolution lamellae (TH-1). (C) Close-up of exsolution lamellae within the magnetite, showing ilmenite and chromite bands (TH-1).

was preformed using a He carrier gas to improve material transport efficiency. The beam spot size was between 30 and 50 μm and had a repetition rate of 4 and 5 Hz. Standard blanks were measured for ~1 minute and calibration was performed using GJ-1 zircon standard, Harvard reference zircon 91500 and Australian Mud Tank carbonitite zircon. Data processing was completed using GLITTER 4.0 for the U-Th-Pb isotope ratios and common lead. Isoplot v. 3.0 was used to plot the Concordia diagram and to calculate the weighted mean U-Pb age (Ludwig, 2003). The results are shown in table 1.

Zircon Hf Isotopes

In situ zircon Hf isotope analyses were carried out using a New Wave UP 213 laser-ablation microprobe, attached to a Nu Plasma multi-collector ICP-MS, at the Institute of Earth Sciences, Academia Sinica in Taipei. Instrumental conditions and data acquisition are similar to Griffin and others (2000). The Nu Plasma MC-ICP-MS features a unique geometry with a fixed detector array of 12 Faraday cups and 3 ion counters. For this study, masses 172, 175, 176, 177, 178, 179 and 180 were simultaneously analyzed and all analyses were carried out in static-collection mode. Data were normalized to $^{179}Hf/^{177}Hf = 0.7325$, using an exponential correction for mass bias. Initial setup of the instrument was done using a 50 ppb solution of AMES Hf metal, which typically yielded a total Hf beam of $10–14 \times 10^{-11}$ A. Isobaric interferences of ^{176}Lu and ^{176}Yb on ^{176}Hf were corrected by measuring the intensities of the interference-free ^{175}Lu and ^{172}Yb isotopes and using appropriate $^{176}Lu/^{175}Lu$ and $^{176}Yb/^{172}Yb$ ratios to calculate $^{176}Lu/^{177}Hf$ and $^{176}Yb/^{177}Hf$ ratios. In the method of Griffin and others (2000) it is assumed that fHf = fYb = fLu (f is he mass fractionation coefficient) and the mass bias obtained for Hf is also applied to the Yb and Lu mass bias correction. With this approach, usually only one Yb isotope is measured (^{172}Yb in this study). Griffin and others (2000) tested this correction method by analyzing solutions of JMC475 spiked with Yb and JMC475 spiked with Lu. The "true" values for $^{172}Yb/^{176}Yb$ and $^{175}Lu/^{176}Lu$ were adjusted to give the "true" $^{176}Hf/^{177}Hf$ of JMC475. The Yb and Lu isotopic compositions derived from the solution analyses were then used to correct the laser analyses. The recommended $^{176}Lu/^{175}Lu$ and $^{176}Yb/^{172}Yb$ ratios of 0.02669 (De BiÈvre and Taylor, 1993) and 0.5865 were used for data reproduction. The accuracy and precision of the method are shown by the analysis of reference zircon (91500, 61308) but are also qualified by noting that the accuracy of the correction procedure was demonstrated for $^{176}Yb/^{177}Hf \leq 0.25$ and $^{176}Lu/^{177}Hf \leq 0.10$. It encompasses the vast majority of typical zircon ($^{176}Yb/^{177}Hf \leq 0.1$ and $^{176}Lu/^{177}Hf \leq 0.002$; Belousova and others, 2002; Griffin and others, 2004; Griffin and others, 2006a) and certainly all of the zircon samples in this study ($^{176}Yb/^{177}Hf \leq 0.1455$ and $^{176}Lu/^{177}Hf \leq 0.0030$; table 1).

The reproducibility of Hf isotope analyses was demonstrated by 28 Hf analyses on the 50 ppb solution of the AMES Hf metal. The mean value for $^{176}Hf/^{177}Hf$ is 0.282152 ± 18 (2σ) is identical to the recommended value of Münker and others (2001) (0.282151 ± 13). The typical 2σ uncertainty on a single analysis of $^{176}Hf/^{177}Hf$ is $6–8 \times 10^{-6}$.

The New Wave UP 213 laser system delivers a beam of 213 nm UV light from a frequency-quintupled (5th harmonic) Nd: YAG laser. Most analyses were carried out with a beam diameter of 55 μm, 5 Hz repetition rate, and energies of ~0.4 mJ/pulse. This resulted in total Hf signals of $1–2.5 \times 10^{-11}$ A, depending on the precise conditions and Hf contents. Typical ablation times were 80 to 120 seconds. The He carrier gas transported the ablated sample from the laser-ablation cell via a mixing chamber where it was mixed with Ar prior to entering the ICP-MS torch. Flux rates for He were about 1 L/min and 0.7 L/min respectively. Laser-ablation analyses were carried out using time-resolved analysis software, in which the signal for each mass and ratio is displayed as a function of time during the analysis. This allows the more stable

Table 1

Results of zircon U/Pb LA-ICP-MS geochronology and zircon Lu-Hf isotopes

Spot	$\frac{^{206}Pb}{^{238}U}$	± 1σ	$\frac{^{207}Pb}{^{235}U}$	± 1σ	Error Correction	$^{206}Pb/^{238}U$ Age (Ma ± 1σ)	$\frac{^{176}Hf}{^{177}Hf}$	± 1σ	$\frac{^{176}Lu}{^{177}Hf}$	± 1σ	$\frac{^{176}Yb}{^{177}Hf}$	± 1σ	I_{Hf}	$\varepsilon Hf_{(T)}$	± 1σ
	TH-1 wt. mean = 264 ± 3 Ma (2σ)						TH-1 wt. mean $\varepsilon Hf_{(T)}$ = +8.1 ± 0.8 (2σ)								
TH-1-01	0.0413	0.0008	0.2897	0.0059	0.9213	261 ± 5	0.282844	0.00001	0.00054	0.00002	0.02425	0.00130	0.282841	+7.7	0.5
TH-1-02	0.4721	0.0089	10.6020	0.2122	0.9400	2493 ± 39									
TH-1-03	0.4817	0.0091	10.8802	0.2194	0.9346	2535 ± 40									
TH-1-04	0.0437	0.0008	0.3072	0.0068	0.8639	276 ± 5	0.282883	0.00004	0.00287	0.00004	0.14558	0.00290	0.282869	+8.7	1.3
TH-1-05	0.0419	0.0008	0.2988	0.0062	0.9108	264 ± 5	0.282854	0.00001	0.00128	0.00010	0.00553	0.00140	0.282848	+7.9	0.4
TH-1-06	0.0424	0.0008	0.2990	0.0064	0.8894	267 ± 5	0.282866	0.00002	0.00208	0.00003	0.01166	0.00250	0.282856	+8.2	0.6
TH-1-07	0.0427	0.0008	0.3013	0.0066	0.8716	269 ± 5	0.282886	0.00001	0.00133	0.00001	0.06584	0.00042	0.282879	+9.0	0.4
TH-1-08	0.0419	0.0008	0.2987	0.0066	0.8695	265 ± 5	0.282871	0.00002	0.00076	0.00001	0.03797	0.00070	0.282867	+8.6	0.6
TH-1-09	0.0417	0.0008	0.2931	0.0065	0.8636	263 ± 5									
TH-1-10	0.0408	0.0008	0.2850	0.0073	0.7608	258 ± 5	0.282847	0.00002	0.00131	0.00005	0.06739	0.00260	0.282841	+7.7	0.6
TH-1-11	0.0412	0.0008	0.2941	0.0069	0.8319	260 ± 5	0.282870	0.00002	0.00007	0.00003	0.04353	0.00250	0.28287	+8.7	0.8
TH-1-12	0.0421	0.0008	0.3022	0.0068	0.8592	266 ± 5	0.282908	0.00002	0.00264	0.00011	0.13507	0.00950	0.282895	+9.6	0.7
TH-1-13	0.0423	0.0008	0.2956	0.0062	0.8968	267 ± 5	0.282828	0.00002	0.00069	0.00001	0.03274	0.00048	0.282825	+7.1	0.7
TH-1-14	0.0414	0.0008	0.2912	0.0081	0.7007	261 ± 5	0.282841	0.00002	0.00068	0.00006	0.03354	0.00290	0.282838	+7.6	0.8
TH-1-15	0.0416	0.0008	0.3071	0.0103	0.5968	263 ± 5	0.282951	0.00003	0.00145	0.00004	0.09016	0.00290	0.282944	+11.3	0.9
TH-1-16	0.0404	0.0008	0.2976	0.0064	0.8828	255 ± 5	0.282770	0.00003	0.00307	0.00007	0.09360	0.00180	0.282755	+4.6	1
TH-1-17	0.0427	0.0008	0.3095	0.0083	0.7268	269 ± 5	0.282831	0.00002	0.00076	0.00003	0.03649	0.00100	0.282827	+7.2	0.5

$T_{(DM\text{-}1)} = (1/0.01865)*\ln((1 + (^{176}Hf/^{177}Hf - 0.28325)/(^{176}Lu/^{177}Hf - 0.0384))$. $T_{(DM\text{-}2)} = (Age/1000) + ((1/0.01865)*\ln(1 + (Hf_i - Hf_{DM(t)})/(0.015 - 0.0384)))$.

portions of the ablation to be selected for analysis, before the data are processed to yield the final results. Background noise was collected for 30 seconds before ablation began. Typical within-run precision (2σ) on the analysis of $^{176}Hf/^{177}Hf$ is ± 0.000030, equivalent to an uncertainty of ~1 epsilon unit.

To evaluate the accuracy and precision of the laser-ablation results, we have repeatedly analyzed two zircon standards, Mud Tank and 91500, both described by Woodhead and Hergt (2005), Griffin and others (2006b), and Weidenbeck and others (1995), respectively. Our long-term result of Mud Tank zircon, yielding 0.282518 ± 48 (2σ; n = 65), is consistent with the reported value of 0.282522 ± 42 (2σ; n = 2335) by Griffin and others (2006b) and also similar to the values given by Woodhead and Hergt (2005) for solution analysis (0.282507 ± 6; n = 5) and LA-MC-ICP-MS analysis (0.282504 ± 44; n = 158). Our result for 91500 is 0.282319 ± 94 (2σ; n = 28) and within the range of the reported values from the literature, although showing a greater spread. Griffin and others (2006b) pointed out that 91500 shows isotopic heterogeneity.

The $\varepsilon Hf_{(T)}$ values are calculated using chondritic ratios of $^{176}Hf/^{177}Hf$ (0.282785) and $^{176}Lu/^{177}Hf$ (0.0336) as derived by Bouvier and others (2008). The ^{176}Lu decay constant of 1.865×10^{-11} yr^{-1} reported by Scherer and others (2001) is used in the calculation. These values were reported relative to $^{176}Hf/^{177}Hf = 0.282163$ for the JMC475 standard. The $^{176}Hf/^{177}Hf$ value of 0.282152 ± 18 was obtained for our AMES Hf metal, which is indistinguishable to the JMC475 standard. The Hf isotopic results are listed in table 1.

X-ray Fluorescence Spectrometry

The rock samples were pulverized in an agate mill and the major oxide concentrations were determined on fused glass discs by WD-XRFS using a Philips PW2400 spectrometer at The University of Hong Kong. The accuracy of the XRF analyses are estimated to be ± 2 percent for major oxides that are present in concentrations >0.5 percent (table 2). Standard reference materials for the major elements were BHVO-2 (basalt), JGB-2 (gabbro) and GSR-1 (granite).

ICP-MS Trace Element Geochemistry

All trace elements were analyzed using a VG Elemental Plasma-Quad Excell inductively coupled plasma mass spectrometry (ICP-MS) at The University of Hong Kong. Sample powders were digested following the technique of Qi and others (2000). For trace element analysis, the standard reference materials were AMH-1 (Mount Hood andesite), GBPG-1 (garnet-biotite plagiogneiss) and OU-6 (Prerhyn slate) (Thompson and others, 1999; Potts and others, 2000, 2001). The precision for the trace element results are better than ± 5 percent (table 2).

TIMS Rb-Sr and Sm-Nd Isotopic Analyses

Approximately 75 to 100 mg of whole-rock powder was dissolved using a mixture of $HF\text{-}HClO_4$ in a Teflon beaker at ~100 °C. In many cases, the same procedures were repeated to ensure the total dissolution of the sample. Strontium and REEs were separated using polyethylene columns with a 5 ml resin bed of AG 50W-X8, 200 to 400 mesh. Neodymium was separated from other REEs using polyethylene columns with a Ln resin as a cation exchange medium. Strontium was loaded on a single Ta-filament with H_3PO_4 and Nd was loaded with H_3PO_4 on a Re-double-filament. $^{143}Nd/^{144}Nd$ ratios were normalized to $^{146}Nd/^{144}Nd = 0.7219$ and $^{87}Sr/^{86}Sr$ ratios to $^{86}Sr/^{88}Sr = 0.1194$. The Sr isotopic ratios and the Nd isotopic ratios were measured using a Finnigan Triton TIMS in the Mass Spectrometry Laboratory, Institute of Earth Sciences, Academia Sinica, Taipei. The $2\sigma_m$ values for all samples are less than 0.000008 for $^{87}Sr/^{86}Sr$ and less than 0.000034 for $^{143}Nd/^{144}Nd$ (table 3). The measured

Table 2

Whole rock geochemical data of the Taihe gabbroic rocks

Sample	GS04-159	GS04-160	GS04-161	GS04-163	GS04-164	GS04-165	GS04-166
Rock	Gabbro	Gabbro	Gabbro	Ore	Gabbro	Gabbro	Gabbro
SiO_2 (wt%)	41.09	41.21	39.93	12.28	40.72	40.11	40.61
TiO_2	2.73	2.88	2.91	11.57	2.95	2.92	2.87
Al_2O_3	21.19	20.25	22.62	10.79	19.52	22.00	22.39
Fe_2O_3	13.88	11.86	13.26	51.34	14.10	13.56	14.43
MnO	0.12	0.11	0.10	0.29	0.13	0.11	0.12
MgO	5.81	5.38	3.95	5.34	6.32	4.65	5.00
CaO	11.77	13.45	12.39	4.23	13.15	12.27	11.90
Na_2O	2.01	2.57	2.45	0.28	2.02	2.51	2.27
K_2O	0.52	0.51	0.54	0.06	0.36	0.63	0.58
P_2O_5	0.12	0.41	0.45	0.04	0.19	0.28	0.13
LOI	0.61	0.56	0.58	2.18	0.62	0.51	0.61
Total	99.85	99.18	99.18	98.39	100.09	99.57	100.91
Mg#	45.3	47.3	37.1	17.1	47.1	40.5	40.7
Sc (ppm)	11	17	10	9	16	11	10
V	144	116	25	2104	153	142	133
Cr	94	32	82	621	68	89	100
Co	58	44	57	185	57	53	52
Ni	146	69	192	427	102	143	136
Cu	244	129	441	1255	242	247	178
Zn	88	80	90	383	101	93	98
Ga	17.4	16.5	18.0	31.4	16.6	17.2	17.3
Rb	16	13	16	1	11	17	16
Sr	1191	1500	1678	586	1329	1557	1507
Y	7.7	8.1	6.4	1.1	5.8	5.5	4.5
Zr	60	30	19	11	23	18	18
Nb	11.1	6.0	4.0	2.2	5.4	3.5	3.3
Cs	0.41	0.23	0.36	0.13	0.35	0.33	0.48
Ba	225	306	289	26	170	300	273
La	9.24	8.21	8.53	1.07	5.79	6.62	6.02
Ce	22.47	21.34	20.36	2.48	14.57	16.27	13.36
Pr	2.84	3.05	2.80	0.28	1.98	2.22	1.86
Nd	11.94	14.95	13.41	1.44	9.33	10.47	8.99
Sm	2.26	3.36	2.73		2.01	2.22	1.60
Eu	1.20	1.64	1.47	0.29	1.26	1.31	1.15
Gd	2.38	3.03	2.67	0.35	2.03	2.21	1.81
Tb	0.34	0.46	0.36	0.05	0.32	0.30	0.26
Dy	1.80	2.20	1.56	0.24	1.40	1.39	1.12
Ho	0.31	0.35	0.31	0.04	0.22	0.24	0.20
Er	0.92	0.96	0.77	0.11	0.65	0.65	0.55
Tm	0.12	0.11	0.09	0.01	0.07	0.08	0.06
Yb	0.68	0.63	0.51	0.07	0.40	0.41	0.35
Lu	0.08	0.09	0.07	0.01	0.06	0.05	0.06
Hf	1.75	1.06	0.65	0.47	0.91	0.66	0.61
Ta	0.82	0.41	0.34	0.23	0.3	0.28	0.27
Th	1.63	0.77	0.31	0.06	0.31	0.3	0.33
U	0.32	0.17	0.09	0.02	0.1	0.07	0.09
$(La/Yb)_N$	9.7	9.3	12.0	11.0	10.4	11.6	12.3
Eu/Eu*	1.6	1.5	1.6	5.9	1.9	1.8	2.1

Table 2
(continued)

Sample	GS04-167	GS04-168	GS04-169	GS04-170	GS04-171	GS04-172	GS04-173
Rock	Ore	Ore	Gabbro	Gabbro	Gabbro	Gabbro	Gabbro
SiO_2 (wt%)	4.38	2.76	43.01	43.65	44.07	46.45	41.38
TiO_2	13.43	14.22	1.97	2.25	1.63	1.29	2.63
Al_2O_3	6.26	5.94	20.53	19.76	22.03	22.13	20.31
Fe_2O_3	68.34	72.72	9.17	10.27	7.38	6.33	11.80
MnO	0.30	0.31	0.10	0.11	0.08	0.09	0.11
MgO	4.97	6.67	5.62	6.14	4.87	5.01	5.51
CaO	1.65	0.27	15.78	15.80	16.22	14.41	14.58
Na_2O	0.48	0.16	2.04	1.78	2.27	2.38	1.88
K_2O	0.04	0.00	0.35	0.46	0.63	0.81	0.41
P_2O_5	0.00	0.00	0.05	0.08	0.11	0.18	0.09
LOI	0.49	0.46	0.43	0.48	0.50	0.93	0.43
Total	100.34	103.53	99.05	100.77	99.80	100.01	99.15
Mg#	12.6	15.4	54.8	54.2	56.6	61.1	48.0
Sc (ppm)	10	11	21	21	19	18	17
V	2516	2550	285	326	212	163	202
Cr	319	57	106	122	83	90	111
Co	203	219	40	43	31	27	47
Ni	470	507	135	106	141	63	109
Cu	937	343	147	122	299	47	131
Zn	437	411	64	72	68	54	92
Ga	35.8	34.9	14.8	15.3	15.3	14.5	15.9
Rb	0	0	15	21	28	33	15
Sr	175	46	1345	1227	1465	1459	1323
Y	0.8	0.5	4.8	5.2	4.8	5.6	4.7
Zr	11	11	11	13	13	16	13
Nb	2.3	2.5	1.1	1.3	1.5	2.8	1.9
Cs	0.13	0.02	0.14	0.19	0.17	0.24	0.17
Ba	5	16	88	131	157	215	112
La	0.72	0.59	2.96	3.42	3.98	5.41	4.05
Ce	1.75	1.38	8.00	9.33	9.77	12.38	10.30
Pr	0.20	0.14	1.26	1.42	1.39	1.80	1.45
Nd	0.97	0.70	6.89	7.47	7.84	9.22	7.75
Sm			1.68	1.82	1.67	1.88	1.63
Eu	0.15	0.13	1.13	1.24	1.23	1.28	1.12
Gd	0.26	0.16	1.54	1.76	1.64	2.04	1.62
Tb	0.04	0.02	0.26	0.27	0.27	0.30	0.24
Dy	0.19	0.11	1.27	1.44	1.33	1.44	1.17
Ho	0.03	0.01	0.22	0.25	0.21	0.25	0.22
Er	0.09	0.06	0.61	0.66	0.55	0.66	0.53
Tm	0.01	0.01	0.06	0.08	0.07	0.08	0.06
Yb	0.06	0.05	0.39	0.40	0.38	0.46	0.38
Lu	0.01	0.01	0.05	0.05	0.05	0.06	0.05
Hf	0.46	0.49	0.56	0.63	0.52	0.7	0.54
Ta	0.28	0.3	0.11	0.12	0.12	0.33	0.17
Th	0.05	0.03	0.09	0.13	0.14	0.41	0.15
U	0.01	0.16	0.03	0.04	0.04	0.12	0.1
$(La/Yb)_N$	8.6	8.5	5.4	6.1	7.5	8.4	7.6
Eu/Eu*	4.1	5.8	2.1	2.1	2.2	2.0	2.1

TABLE 2
(continued)

Sample	GS04-174	TH-1	Parent	Parent	Parent	AMH-1	GBPG-1	OU-6
Rock	Gabbro	Ore	Taihe	Baima	Panzhihua	m.v.	m.v.	m.v.
SiO_2 (wt%)	45.41	16.66	50.45	44.64	49.18			
TiO_2	1.70	8.79	2.61	3.48	2.94			
Al_2O_3	19.03	11.26	12.36	13.79	11.53			
Fe_2O_3	8.27	40.57	12.19	16.41	12.67			
MnO	0.10	0.28	0.20	0.22	0.19			
MgO	7.23	7.10	7.44	6.95	8.74			
CaO	16.93	5.74	9.95	10.18	10.54			
Na_2O	1.65	0.31	2.61	2.40	2.28			
K_2O	0.28	0.04	1.41	1.09	1.12			
P_2O_5	0.05	0.02	0.30	0.35	0.31			
LOI	0.35	1.00	0.5	0.5	0.5			
Total	100.99	91.77	100	100	100			
Mg#	63.4	25.7	54.8	45.6	57.8			
Sc (ppm)	26	18				14.8	16.4	21.2
V	246	1573				106.9	91.9	117.6
Cr	134	19040				41.6	175.1	68.6
Co	36	115	54	52	54	19.9	19.7	27.2
Ni	120	429	115	85	115	34.3	54.9	36.6
Cu	116	109				34.0	32.4	50.9
Zn	63	248				67.1	76.0	105.1
Ga	14.1	36.0				20.28	20.29	24.93
Rb	12	0.8				17.6	53.5	113.8
Sr	1188	447	550	780	548	547.5	353.7	126
Y	6.1	3.0				14.7	18.0	25.3
Zr	13	18				144.0	259.6	174.8
Nb	1.0	1.5	24	31	30.8	7.79	9.27	13.23
Cs	0.18	0.12				0.24	0.31	7.81
Ba	79	31	475	590	498	319.5	893.9	472.5
La	3.18	0.88				16.23	50.82	33.56
Ce	9.03	3.31				35.44	109.10	81.18
Pr	1.36	0.51				4.20	11.98	8.16
Nd	8.09	3.14				16.14	42.11	30.77
Sm	2.09	098				3.45	6.78	5.86
Eu	1.32	0.49				1.20	1.77	1.43
Gd	1.90	0.13				3.54	4.90	5.53
Tb	0.32	1.00				0.55	0.78	0.91
Dy	1.51	0.68				2.97	3.20	5.13
Ho	0.24	0.12				0.55	0.63	1.01
Er	0.66	0.26				1.77	2.30	3.25
Tm	0.08	0.03				0.23	0.31	0.47
Yb	0.42	0.18				1.46	2.11	3.06
Lu	0.05	0.02				0.23	0.31	0.46
Hf	0.66	0.52				3.81	6.21	4.99
Ta	0.09	0.16	1.6	1.7	2.1	0.60	0.40	0.98
Th	0.09	0.04				2.27	10.99	10.20
U	0.04	0.01				0.88	0.88	1.95
$(La/Yb)_N$	5.4	3.6						
Eu/Eu*	2.0	2.4						

LOI = loss on ignition; Mg# = $100*[Mg^{2+}/Mg^{2+} + Fe^{2+}]$ where FeOt = 0.8998*Fe2O3t; $(La/Yb)_N$ is normalized to chondrite values of Sun and McDoungh (1989). $Eu/Eu^* = [2*Eu_N/(Sm_N + Gd_N)]$. m.v. = mean value.

TABLE 3

Whole rock Sr and Nd isotopic data for the layered gabbro

Sample	Rock	Rb (ppm)	Sr (ppm)	$\frac{^{87}Rb}{^{86}Sr}$	$\frac{^{87}Sr}{^{86}Sr}$	±2σm	I_{Sr}	Model Age (Ma)	Sm (ppm)	Nd (ppm)	$\frac{^{147}Sm}{^{144}Nd}$	$\frac{^{143}Nd}{^{144}Nd}$	±2σm	εNd(0)	εNd(T)	f (Sm/Nd)	TDM-1
GS04-161	Gabbro	15.8	1678	0.027	0.705143	6	0.70504	2920	2.73	13.4	0.1231	0.512660	6	0.4	+2.9	-0.37	825
GS04-165	Gabbro	16.7	1557	0.031	0.705158	8	0.70504	2583	2.22	10.5	0.1282	0.512650	34	0.2	+2.5	-0.35	892
GS04-169	Gabbro	14.5	1345	0.031	0.705164	7	0.70505	2596	1.68	6.89	0.1474	0.512710	6	1.4	+3.0	-0.25	1011
GS04-172	Gabbro	32.9	1459	0.065	0.705277	7	0.70504	1370	1.88	9.22	0.1233	0.512681	6	0.8	+3.3	-0.37	791

Rb, Sr, Sm, and Nd concentrations were obtained by ICP-MS and precisions better than ±2%. The results of isotopic measurements for Sr and Nd reference materials are NBS-987 (Sr) = 0.710248 ± 3 (2σm). JMC (Nd) = 0.511813 ± 10 (2σm). f(Sm/Nd) is defined as $(({}^{147}Sm/{}^{144}Nd)/0.1967 - 1)$. $\varepsilon Nd_{(T)}$ is calculated using an approximate equation of $\varepsilon Nd_{(T)} = \varepsilon Nd_{(0)} - Q*f*T$; in which Q = 25.1 Ga^{-1}, f = f(Sm/Nd), T age = 0.26 Ga. $T_{DM} - 1 = (1/\lambda)*\ln[1 + (({}^{143}Nd/{}^{144}Nd)_m - 0.51315)/(({}^{147}Sm/{}^{144}Nd)_m - 0.2137)]$; $\lambda = 0.00654\ Ga^{-1}$. The assumed $I_{Sr} = 0.704$ for the model age.

TABLE 4

EPMA analyses of the olivine from the Taihe layered gabbroic rocks

Sample No.	N1-109	N1-147	N1-148	N1-149	N1-150	N1-110	N1-123	N1-124	N1-125	N1-126
SiO_2 (wt%)	39.11	39.32	39.01	39.74	37.47	39.56	38.64	39.02	39.62	39.72
TiO_2	0.02	0.00	0.00	0.00	0.01	0.03	0.02	0.02	0.04	0.09
Al_2O_3	0.02	0.07	0.00	0.07	0.01	0.00	0.00	0.02	0.01	0.07
Cr_2O_3	0.00	0.01	0.00	0.00	0.00	0.01	0.00	0.00	0.01	0.00
FeO	23.02	22.81	22.70	22.89	23.07	22.58	22.67	22.80	22.28	22.90
MnO	0.34	0.36	0.37	0.38	0.33	0.33	0.33	0.27	0.24	0.37
MgO	39.73	39.60	39.47	39.98	40.30	39.83	39.44	39.93	39.38	39.39
NiO	0.19	0.10	0.14	0.09	0.05	0.00	0.06	0.04	0.08	0.07
CaO	0.00	0.01	0.04	0.04	0.03	0.00	0.04	0.02	0.03	0.11
Na_2O	0.01	0.01	0.02	0.00	0.00	0.00	0.00	0.00	0.00	0.01
K_2O	0.00	0.01	0.00	0.00	0.00	0.00	0.00	0.00	0.00	0.00
Total	102.45	102.30	101.74	103.18	101.27	102.33	101.21	102.11	101.67	102.73
Cations on the Basis of 4O										
Si	1.4930	1.5004	1.4977	1.5022	1.4540	1.5055	1.4918	1.4919	1.5151	1.5082
Ti	0.0007	0.0000	0.0000	0.0000	0.0002	0.0007	0.0007	0.0007	0.0010	0.0025
Al	0.0009	0.0031	0.0000	0.0029	0.0002	0.0000	0.0000	0.0009	0.0003	0.0032
Cr	0.0000	0.0002	0.0000	0.0000	0.0000	0.0003	0.0000	0.0000	0.0002	0.0000
Fe^{2+}	0.7347	0.7275	0.7288	0.7234	0.7485	0.7183	0.7319	0.7287	0.7122	0.7271
Mn	0.0110	0.0115	0.0119	0.0120	0.0108	0.0107	0.0109	0.0086	0.0078	0.0118
Mg	2.2593	2.2509	2.2573	2.2514	2.3291	2.2581	2.2683	2.2746	2.2435	2.2281
Ni	0.0057	0.0031	0.0043	0.0028	0.0016	0.0000	0.0020	0.0011	0.0024	0.0022
Ca	0.0000	0.0005	0.0017	0.0015	0.0013	0.0000	0.0018	0.0007	0.0012	0.0044
Na	0.0010	0.0010	0.0014	0.0000	0.0000	0.0000	0.0000	0.0000	0.0000	0.0004
K	0.0000	0.0006	0.0000	0.0002	0.0000	0.0000	0.0001	0.0000	0.0000	0.0000
Total	4.506	4.499	4.503	4.496	4.546	4.494	4.508	4.507	4.484	4.488
Fo	75.5	75.6	75.6	75.6	75.6	75.9	75.6	75.7	75.9	75.3
Fa	24.5	24.4	24.4	24.3	24.3	24.1	24.4	24.3	24.1	24.6

Mineral symbols: Fo = forsterite component; Fa = fayalite component.

isotopic ratios for JMC Nd standard is 0.511813 ± 0.000010 ($2\sigma_m$) and NBS987-Sr is 0.710248 ± 0.00001 ($2\sigma_m$).

RESULTS

Mineral Chemistry

Olivine crystals have forsterite (Fo) percentages between 75 to 76 (table 4) and are similar to the olivine from the marginal and lower zones of the Panzhihua intrusion (Fo_{82-71}) and the upper oxide zone of the Baima gabbro (Fo_{76-72}) (Pang and others, 2009). The Fo values indicate a minimum parental magma Mg# of 49 (Roeder and Emslie, 1970). Individual crystals are commonly reversely zoned with higher Mg rims, probably reflecting sub-solidus cation exchange with the surrounding oxide minerals. The plagioclase compositions in GS04-174 range from An_{84} to An_{70} (table 5). The clinopyroxene crystals are diopside-augite and have a compositional range of $Wo_{49-50}En_{42-40}Fs_{11-8}$. The TiO_2 concentration varies between 1.8 and 2.0 weight percent (table 6). There is substantial oxidation-exsolution of the oxide minerals so the magnetite analyses are nearly pure end-member compositions with $TiO_2 < 0.3$ weight percent. There are also oxidation-exsolution lamellae of spinel (chromite and pleonaste) within the magnetite. The ilmenite lamellae have low MgO (<0.1wt%) and

TABLE 5

EPMA analyses of the plagioclase from the Taihe layered gabbroic rocks

Sample	N1-131	N1-132	N1-134	N1-138	N11-93
SiO_2 (wt%)	48.49	49.06	48.68	45.52	45.26
TiO_2	0.06	0.06	0.01	0.05	0.11
Al_2O_3	33.20	32.18	32.70	30.60	30.45
Cr_2O_3	0.00	0.00	0.00	0.01	0.00
FeO	0.30	0.35	0.33	1.26	0.82
MnO	0.00	0.00	0.02	0.00	0.05
MgO	0.01	0.03	0.03	0.00	0.02
NiO	0.06	0.06	0.01	0.03	0.09
CaO	16.69	13.35	16.59	19.73	20.52
Na_2O	1.88	2.92	2.00	2.03	1.90
K_2O	0.03	0.29	0.00	0.00	0.00
Total	100.71	98.30	100.36	99.21	99.22
Cations on the Basis of 32O					
Si	8.828	9.086	8.890	8.600	8.5612
Ti	0.008	0.008	0.002	0.006	0.0158
Al	7.123	7.023	7.038	6.812	6.7875
Cr	0.000	0.000	0.000	0.001	0.0000
Fe^{2+}	0.045	0.055	0.050	0.198	0.1295
Mn	0.000	0.000	0.002	0.000	0.0083
Mg	0.002	0.008	0.007	0.001	0.0065
Ni	0.008	0.009	0.001	0.005	0.0135
Ca	3.254	2.648	3.246	3.992	4.1582
Na	0.662	1.048	0.707	0.742	0.6972
K	0.007	0.068	0.000	0.000	0.0000
Total	19.937	19.953	19.943	20.358	20.3779
An	82.9	70.3	82.1	84.3	85.6
Ab	16.9	27.8	17.9	15.7	14.4
Or	0.2	1.8	0.0	0.0	0.0

Mineral symbols: An = anorthite component; Ab = albite component; Or = orthoclase component.

Al_2O_3 (<0.1 wt%) with MnO concentrations between 1.3 and 1.6 weight percent. The analytical results for the oxide minerals can be found in tables 7 and 8.

Zircon U-Pb Age and Hf Isotopic Ratios

Zircon crystals from sample TH-1, collected from the middle portion of the Taihe open pit mine at 27°54′24′N, 102°07′34″E, show typical igneous zonation and have fragmented, anhedral and euhedral textures. Analyses of fifteen individual zircon crystals form a single age group and yield a mean $^{206}U/^{238}Pb$ age of 264 ± 3 Ma with a mean square of weighted deviates (MSWD) of 1.05 (fig. 4). Two zircon grains produced ages of ~2500 Ma indicating either sample contamination or that they are xenocrysts from the Yangtze cratonic basement (table 1). The zircons were analyzed for their Hf isotope compositions at the same locations as their U-Pb ages. A total of 14 spot analyses from sample TH-1 produced a range of I_{Hf} (0.282755 to 0.282944) and $\varepsilon Hf_{(T)}$ (+4.6 to +11.3) values. The weighted average $\varepsilon Hf_{(T)}$ value is +8.1 ± 0.8.

TABLE 6

EPMA analyses of the clinopyroxene from the Taihe layered gabbroic rocks

Sample	N11-75	N11-79	N11-80	N11-81	N11-82	N11-84	N11-91	N6-95	N1-135	N1-136
SiO_2 (wt%)	48.88	49.38	43.36	49.27	49.16	49.55	49.64	49.17	49.36	49.29
TiO_2	1.89	1.84	1.94	1.76	1.87	1.87	1.91	2.08	1.96	1.98
Al_2O_3	5.96	5.35	5.50	5.21	5.12	4.80	5.19	5.59	5.63	5.47
Cr_2O_3	0.15	0.10	0.16	0.12	0.07	0.10	0.07	0.03	0.06	0.10
FeO	6.03	4.82	4.96	5.60	6.35	5.82	4.75	5.07	6.68	6.56
MnO	0.17	0.15	0.10	0.14	0.11	0.15	0.15	0.10	0.18	0.18
MgO	14.01	14.02	13.84	14.33	13.90	13.79	13.80	13.69	13.57	13.48
NiO	0.06	0.05	0.00	0.01	0.07	0.13	0.11	0.04	0.00	0.00
CaO	23.06	23.60	22.81	23.29	23.23	23.01	23.11	22.98	22.81	23.22
Na_2O	0.34	0.42	0.38	0.37	0.29	0.28	0.33	0.40	0.44	0.35
K_2O	0.01	0.00	0.00	0.00	0.00	0.00	0.00	0.01	0.00	0.00
Total	100.56	99.73	93.05	100.10	100.16	99.50	99.04	99.16	100.67	100.64
Cations on the Basis of 6O										
Si	1.8055	1.8304	1.7438	1.8248	1.8254	1.8457	1.8475	1.8308	1.8227	1.8226
Ti	0.0525	0.0513	0.0586	0.0491	0.0523	0.0524	0.0533	0.0583	0.0544	0.0550
Al	0.2592	0.2335	0.2607	0.2274	0.2240	0.2106	0.2275	0.2452	0.2450	0.2381
Cr	0.0045	0.0029	0.0050	0.0035	0.0020	0.0030	0.0021	0.0010	0.0017	0.0030
Fe^{2+}	0.1862	0.1495	0.1668	0.1733	0.1970	0.1813	0.1478	0.1579	0.2062	0.2027
Mn	0.0052	0.0047	0.0034	0.0045	0.0034	0.0048	0.0047	0.0032	0.0055	0.0056
Mg	0.7706	0.7742	0.8291	0.7908	0.7688	0.7652	0.7650	0.7594	0.7463	0.7426
Ni	0.0018	0.0015	0.0000	0.0002	0.0020	0.0037	0.0033	0.0011	0.0000	0.0000
Ca	0.9122	0.9368	0.9823	0.9240	0.9239	0.9180	0.9212	0.9163	0.9021	0.9194
Na	0.0243	0.0304	0.0299	0.0263	0.0210	0.0201	0.0234	0.0290	0.0314	0.0252
K	0.0007	0.0000	0.0000	0.0000	0.0000	0.0000	0.0000	0.0003	0.0000	0.0000
Total	4.0227	4.0152	4.0797	4.0238	4.0198	4.0051	3.9960	4.0024	4.0152	4.0144
En	41.2	41.6	41.9	41.9	40.7	41.0	41.7	41.4	40.2	39.8
Fs	10.0	8.0	8.4	9.2	10.4	9.7	8.1	8.6	11.1	10.9
Wo	48.8	50.4	49.7	48.9	48.9	49.2	50.2	50.0	48.6	49.3

Mineral symbols: En = enstatite component; Fs = ferrosilite component; Wo = wollastonite component.

Whole-Rock Geochemistry

Sixteen samples from two sites of the cumulate layered gabbro were collected from the operating open pit mine at Taihe. Twelve of the samples are gabbros while four are magnetite-rich gabbros. All samples have low (<2.1 wt%) loss on ignition (LOI) suggesting that there was limited deuteric alteration of the samples (table 2). Although the samples have similar major element chemistry, the gabbros from the eastern locality have higher Mg# (Mg# = 48 to 63) than those in the western locality (Mg# = 37 to 47). The differences in Mg# are attributed to the amount of oxide minerals, as the Fe_2O_3t and TiO_2 contents are higher in the west (Fe_2O_3t = 11.9 to 14.4 wt%; TiO_2 = 2.7 to 2.9 wt%) than in the east (Fe_2O_3t = 6.3 to 11.8 wt%; TiO_2 = 1.3 to 2.6 wt%). The whole-rock compositions are directly related to the ratio of silicate minerals to oxide minerals. For example, the samples in the western locality have lower

Table 7

EPMA analyses of the ilmenite from the Taihe layered gabbroic rocks

Sample	N12-3	N12-7	N12-8	N12-13	N12-15	N12-17	N12-18	N12-25	N12-26	N12-27	N12-28	N12-29	N12-30	N11-37
SiO_2 (wt%)	0.01	0.00	0.05	0.15	0.00	0.00	0.07	0.02	0.03	0.03	0.04	0.04	0.00	0.01
TiO_2	50.20	50.99	50.09	52.20	50.80	52.20	50.22	49.99	49.45	50.51	50.59	50.89	49.51	51.11
Al_2O_3	0.00	0.02	0.01	0.03	0.00	0.00	0.00	0.04	0.07	0.04	0.00	0.02	0.04	0.00
Cr_2O_3	0.00	0.00	0.02	0.00	0.01	0.00	0.00	0.00	0.00	0.00	0.00	0.00	0.00	0.00
FeOT	47.92	47.37	47.29	46.07	48.83	46.67	46.77	48.44	48.51	48.74	47.63	48.37	48.59	47.88
NiO	0.02	0.01	0.00	0.08	0.00	0.05	0.01	0.00	0.03	0.00	0.09	0.06	0.04	0.00
MnO	1.29	1.47	1.49	1.39	1.52	1.58	1.34	1.42	1.47	1.51	1.52	1.57	1.52	1.43
MgO	0.10	0.03	0.02	0.11	0.04	0.02	0.08	0.08	0.08	0.05	0.03	0.07	0.00	0.04
CaO	0.02	0.03	0.07	0.13	0.02	0.04	0.00	0.04	0.04	0.00	0.03	0.00	0.00	0.03
Total	99.55	99.91	99.03	100.15	101.21	100.55	98.48	100.03	99.68	100.89	99.95	101.01	99.70	100.49
Fe_2O_3	4.76	3.44	4.25	0.88	5.31	1.63	3.36	5.67	6.35	5.45	4.24	4.80	6.28	3.86
FeO	43.64	44.28	43.47	45.28	44.06	45.20	43.74	43.35	42.80	43.84	43.82	44.05	42.94	44.41
Total	100.03	100.26	99.45	100.24	101.75	100.71	98.82	100.60	100.32	101.43	100.37	101.49	100.34	100.88
Si	0.000	0.000	0.001	0.004	0.000	0.000	0.002	0.000	0.001	0.001	0.001	0.001	0.000	0.000
Al	0.000	0.001	0.000	0.001	0.000	0.000	0.000	0.001	0.002	0.001	0.000	0.001	0.001	0.000
Fe^{3+}	0.090	0.065	0.081	0.017	0.099	0.031	0.065	0.107	0.121	0.102	0.080	0.090	0.119	0.073
Ti	0.954	0.967	0.958	0.987	0.950	0.985	0.966	0.945	0.938	0.947	0.959	0.954	0.940	0.963
Cr	0.000	0.000	0.000	0.000	0.000	0.000	0.000	0.000	0.000	0.000	0.000	0.000	0.000	0.000
Fe^{2+}	0.923	0.934	0.924	0.953	0.916	0.948	0.936	0.912	0.903	0.915	0.923	0.918	0.906	0.931
Ni	0.000	0.000	0.000	0.002	0.000	0.001	0.000	0.000	0.001	0.000	0.002	0.001	0.001	0.000
Mn	0.028	0.031	0.032	0.030	0.032	0.033	0.029	0.030	0.031	0.032	0.033	0.033	0.033	0.030
Mg	0.004	0.001	0.001	0.004	0.001	0.001	0.003	0.003	0.003	0.002	0.001	0.002	0.000	0.002
Ca	0.001	0.001	0.002	0.003	0.000	0.001	0.000	0.001	0.001	0.000	0.001	0.000	0.000	0.001
Total	2.000	2.000	2.000	2.000	2.000	2.000	2.000	2.000	2.000	2.000	2.000	2.000	2.000	2.000

Table 7
(continued)

Sample	N11-38	N11-39	N11-40	N11-41	N11-42	N11-46	N11-48	N11-53	N11-56	N11-61	N11-65	N11-66	N11-67	N1-115	N2-139
SiO_2 (wt%)	0.00	0.05	0.01	0.00	0.01	0.00	0.16	0.00	0.00	0.00	0.00	0.08	0.00	0.01	0.07
TiO_2	51.57	49.84	50.20	50.28	50.06	50.86	51.14	51.02	52.15	51.25	49.91	50.59	51.13	53.20	50.58
Al_2O_3	0.02	0.02	0.02	0.05	0.01	0.00	0.01	0.00	0.00	0.00	0.00	0.08	0.01	0.00	0.01
Cr_2O_3	0.00	0.00	0.00	0.00	0.00	0.00	0.00	0.00	0.00	0.00	0.00	0.00	0.00	0.00	0.00
FeOT	47.26	48.08	48.82	49.47	48.37	47.78	47.78	47.35	45.67	47.62	49.06	46.56	47.45	46.99	48.38
NiO	0.01	0.00	0.01	0.00	0.04	0.00	0.10	0.03	0.00	0.00	0.04	0.07	0.02	0.13	0.00
MnO	1.29	1.36	1.34	1.35	1.27	1.13	1.30	1.14	1.35	1.25	1.20	1.33	1.57	1.37	1.23
MgO	0.00	0.02	0.01	0.03	0.08	0.05	0.04	0.01	0.02	0.03	0.02	0.00	0.06	0.05	0.01
CaO	0.07	0.12	0.03	0.00	0.00	0.00	0.01	0.01	0.01	0.03	0.03	0.00	0.00	0.00	0.10
Total	100.21	99.49	100.43	101.17	99.84	99.82	100.53	99.55	99.20	100.19	100.25	98.71	100.24	101.74	100.37
Fe_2O_3	2.55	5.30	5.66	6.30	5.35	3.65	3.45	2.98	0.22	3.22	6.11	2.66	3.55	0.83	4.67
FeO	44.97	43.32	43.73	43.80	43.56	44.50	44.68	44.67	45.48	44.72	43.56	44.17	44.26	46.24	44.18
Total	100.47	100.03	101.00	101.80	100.38	100.19	100.88	99.85	99.23	100.51	100.87	98.98	100.60	101.83	100.84
Si	0.000	0.001	0.000	0.000	0.000	0.000	0.004	0.000	0.000	0.000	0.000	0.002	0.000	0.000	0.002
Al	0.001	0.001	0.000	0.002	0.000	0.000	0.000	0.000	0.000	0.000	0.000	0.002	0.000	0.000	0.000
Fe^{3+}	0.048	0.101	0.107	0.118	0.102	0.069	0.065	0.057	0.004	0.061	0.115	0.051	0.067	0.015	0.088
Ti	0.976	0.948	0.946	0.940	0.949	0.965	0.963	0.972	0.998	0.969	0.942	0.971	0.966	0.992	0.954
Cr	0.000	0.000	0.000	0.000	0.000	0.000	0.000	0.000	0.000	0.000	0.000	0.000	0.000	0.000	0.000
Fe^{2+}	0.946	0.916	0.916	0.911	0.918	0.939	0.936	0.946	0.968	0.941	0.915	0.943	0.930	0.959	0.927
Ni	0.000	0.000	0.000	0.000	0.001	0.000	0.002	0.001	0.000	0.000	0.001	0.001	0.000	0.003	0.000
Mn	0.028	0.029	0.028	0.028	0.027	0.024	0.028	0.024	0.029	0.027	0.026	0.029	0.034	0.029	0.026
Mg	0.000	0.001	0.000	0.001	0.003	0.002	0.001	0.000	0.001	0.001	0.001	0.000	0.002	0.002	0.000
Ca	0.002	0.003	0.001	0.000	0.000	0.000	0.000	0.000	0.000	0.001	0.001	0.000	0.000	0.000	0.003
Total	2.000	2.000	2.000	2.000	2.000	2.000	2.000	2.000	2.000	2.000	2.000	2.000	2.000	2.000	2.000

Mineral symbols: TFeO = total Fe^{2+}.

Table 8

EPMA analyses of the magnetite from the Taihe layered gabbroic rocks

Sample	N12-5	N12-6	N12-9	N12-10	N12-11	N12-12	N12-14	N12-19	N12-20	N12-21	N12-22	N12-23
SiO_2 (wt%)	0.06	0.00	0.00	0.06	0.03	0.00	0.03	0.02	0.02	0.04	0.06	0.01
TiO_2	0.21	0.10	0.28	0.16	0.31	0.19	0.30	0.21	0.13	0.06	0.08	0.25
Al_2O_3	0.18	0.11	0.26	0.24	0.19	0.52	0.77	0.09	0.39	0.08	0.06	0.19
Cr_2O_3	0.19	0.11	0.11	0.13	0.09	0.07	0.11	0.13	0.09	0.05	0.08	0.18
FeOT	92.84	91.58	92.30	91.52	91.92	91.89	90.97	92.64	92.77	92.23	92.55	92.70
NiO	0.02	0.26	0.09	0.12	0.13	0.14	0.04	0.10	0.09	0.05	0.11	0.08
MnO	0.00	0.00	0.00	0.00	0.00	0.00	0.00	0.00	0.00	0.00	0.00	0.00
MgO	0.01	0.00	0.02	0.00	0.00	0.00	0.04	0.03	0.00	0.00	0.01	0.00
Total	93.50	92.15	93.05	92.21	92.67	92.80	92.27	93.21	93.48	92.51	92.94	93.40
Fe_2O_3	68.26	67.80	67.92	67.41	67.59	67.63	66.57	68.32	68.37	68.17	68.39	68.22
FeO	31.42	30.57	31.19	30.86	31.10	31.03	31.07	31.16	31.25	30.89	31.01	31.32
Total	100.34	98.95	99.85	98.97	99.44	99.58	98.94	100.06	100.33	99.34	99.79	100.23
Si	0.002	0.000	0.000	0.002	0.001	0.000	0.001	0.001	0.001	0.001	0.002	0.000
Al^{vi}	0.008	0.005	0.012	0.011	0.009	0.024	0.035	0.004	0.017	0.004	0.003	0.009
Fe^{3+}	1.969	1.986	1.969	1.972	1.968	1.963	1.941	1.978	1.971	1.989	1.986	1.971
Ti	0.006	0.003	0.008	0.005	0.009	0.005	0.009	0.006	0.004	0.002	0.002	0.007
Cr	0.006	0.003	0.003	0.004	0.003	0.002	0.003	0.004	0.003	0.002	0.002	0.005
Fe^{2+}	1.007	0.995	1.005	1.003	1.006	1.001	1.007	1.003	1.001	1.001	1.001	1.005
Ni	0.001	0.008	0.003	0.004	0.004	0.004	0.001	0.003	0.003	0.002	0.003	0.002
Mn	0.000	0.000	0.000	0.000	0.000	0.000	0.000	0.000	0.000	0.000	0.000	0.000
Mg	0.000	0.000	0.001	0.000	0.000	0.000	0.002	0.001	0.000	0.000	0.000	0.000
Total	3.000	3.000	3.000	3.000	3.000	3.000	3.000	3.000	3.000	3.000		3.000

Table 8
(continued)

Sample	N12-24	N11-35	N11-43	N11-44	N11-45	N11-54	N11-55	N11-57	N11-58	N11-59	N11-63	N11-68
SiO_2 (wt%)	0.06	0.01	0.01	0.04	0.00	0.00	0.01	0.09	0.04	0.06	0.00	0.05
TiO_2	0.29	0.07	0.18	0.37	0.20	0.14	0.09	0.10	0.07	0.14	0.11	0.25
Al_2O_3	0.39	0.14	0.26	0.83	0.02	0.38	0.33	0.29	0.34	0.37	0.20	0.54
Cr_2O_3	0.12	0.08	0.19	0.11	0.06	0.03	0.08	0.06	0.08	0.09	0.16	0.14
FeOT	92.29	92.91	92.11	90.54	93.25	92.24	90.89	92.97	92.95	90.97	90.11	91.81
NiO	0.11	0.13	0.17	0.10	0.11	0.07	0.02	0.04	0.19	0.00	0.15	0.11
MnO	0.00	0.00	0.00	0.00	0.00	0.00	0.00	0.00	0.00	0.00	0.00	0.00
MgO	0.00	0.01	0.00	0.00	0.06	0.00	0.00	0.01	0.01	0.00	0.00	0.00
Total	93.26	93.35	92.92	91.99	93.71	92.86	91.43	93.56	93.68	91.63	90.73	92.90
Fe_2O_3	67.73	68.72	67.91	66.12	68.94	68.00	67.02	68.46	68.64	66.88	66.57	67.34
FeO	31.35	31.07	31.01	31.04	31.22	31.06	30.59	31.36	31.19	30.79	30.22	31.22
Total	100.04	100.24	99.72	98.62	100.62	99.68	98.14	100.42	100.56	98.33	97.40	99.65
Si	0.002	0.000	0.000	0.001	0.000	0.000	0.000	0.003	0.002	0.002	0.000	0.002
Al^{vi}	0.018	0.006	0.012	0.038	0.001	0.017	0.015	0.013	0.015	0.017	0.009	0.025
Fe^{3+}	1.958	1.986	1.971	1.934	1.985	1.974	1.976	1.972	1.975	1.967	1.979	1.953
Ti	0.008	0.002	0.005	0.011	0.006	0.004	0.003	0.003	0.002	0.004	0.003	0.007
Cr	0.003	0.002	0.006	0.003	0.002	0.001	0.003	0.002	0.002	0.003	0.005	0.004
Fe^{2+}	1.007	0.998	1.000	1.009	0.999	1.002	1.002	1.004	0.997	1.006	0.998	1.006
Ni	0.003	0.004	0.005	0.003	0.003	0.002	0.001	0.001	0.006	0.000	0.005	0.003
Mn	0.000	0.000	0.000	0.000	0.000	0.000	0.000	0.000	0.000	0.000	0.000	0.000
Mg	0.000	0.001	0.000	0.000	0.003	0.000	0.000	0.001	0.000	0.000	0.000	0.000
Total	3.000	3.000	3.000	3.000	3.000	3.000	3.000	3.000	3.000	3.000	3.000	3.000

Mineral symbols: TFeO = total Fe^{2+}.

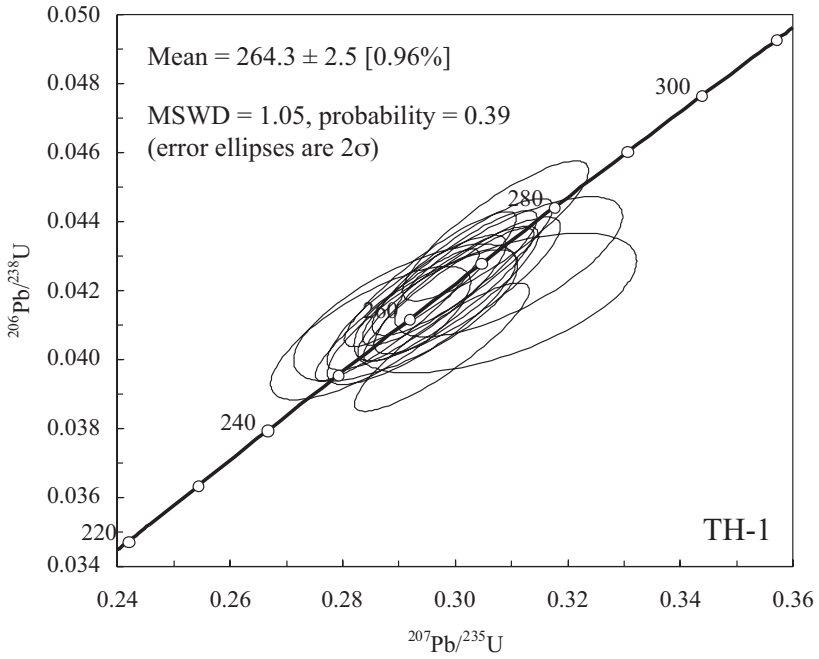

Fig. 4. Concordia plot of the zircon U-Pb LA-ICP-MS results for Taihe gabbro (TH-1).

SiO_2, CaO and MgO than the eastern locality, suggesting that the amount of clinopyroxene is different. The four magnetite-rich samples are composed of at least 75 percent oxide minerals as they contain ≤16.7 weight percent SiO_2 and have between 40.5 and 72.7 weight percent Fe_2O_3t. Some of the bulk-rock ore compositions (GS04-167 and −168) indicate that the samples are nearly 100 percent Ti-rich magnetite as their SiO_2 contents are <4 weight percent. The major elemental compositions of the gabbros, in some cases, appear to form a continuous trend (for example, Fe_2O_3t and TiO_2) with the data from the Taihe granitic rocks. However there are distinct SiO_2 and alkali gaps between the two rock types (fig. 5).

The gabbros have variable amounts of Sc (9-26 ppm), Ni (63-429 ppm), Co (27-185 ppm), Cu (47-1255 ppm), V (25-2104 ppm), Cr (32-19040 ppm), and Sr (586-1678 ppm) and low concentrations of Rb (<33 ppm), Zr (<60 ppm) and Nb (<11.1 ppm). Sample TH-1 contains substantially higher Cr, Ni, V and Cu than the other ore samples. The higher refractory elements are probably related to the concentration of chromite lamellae (fig. 3) or chromite crystals. Similar to the major elements, the trace elements of the cumulate gabbroic rocks and the granitic plutonic rocks show a bimodal distribution (fig. 6). Primitive mantle normalized incompatible trace element patterns show distinct positive anomalies of Sr and Ti and troughs of Th to Ce and Hf and Zr (fig. 7A). The magnetite-rich samples show very depleted patterns although they have positive Sr and Ti anomalies. All rocks have LREE enriched patterns with $(La/Yb)_N$ ratios between 5.4 and 12.3 and Eu-anomalies ($Eu/Eu^* = ([2*Eu_N/(Sm_N+Gd_N)])$ ranging from 1.5 to 5.9 (fig. 8A).

Whole-rock radiogenic Sr and Nd isotopes were determined for four samples from the layered gabbro body (table 3). Their I_{Sr} and $\varepsilon Nd_{(T)}$ values have been calculated to the mean zircon LA-ICP-MS U-Pb age. The I_{Sr} values of the gabbros are identical having a narrow range from 0.70504 to 0.70505. The $^{144}Nd/^{143}Nd_{initial}$ values also have a narrow range from 0.512431 to 0.512472 with $\varepsilon Nd_{(T)}$ ratios of +2.5 to +3.3.

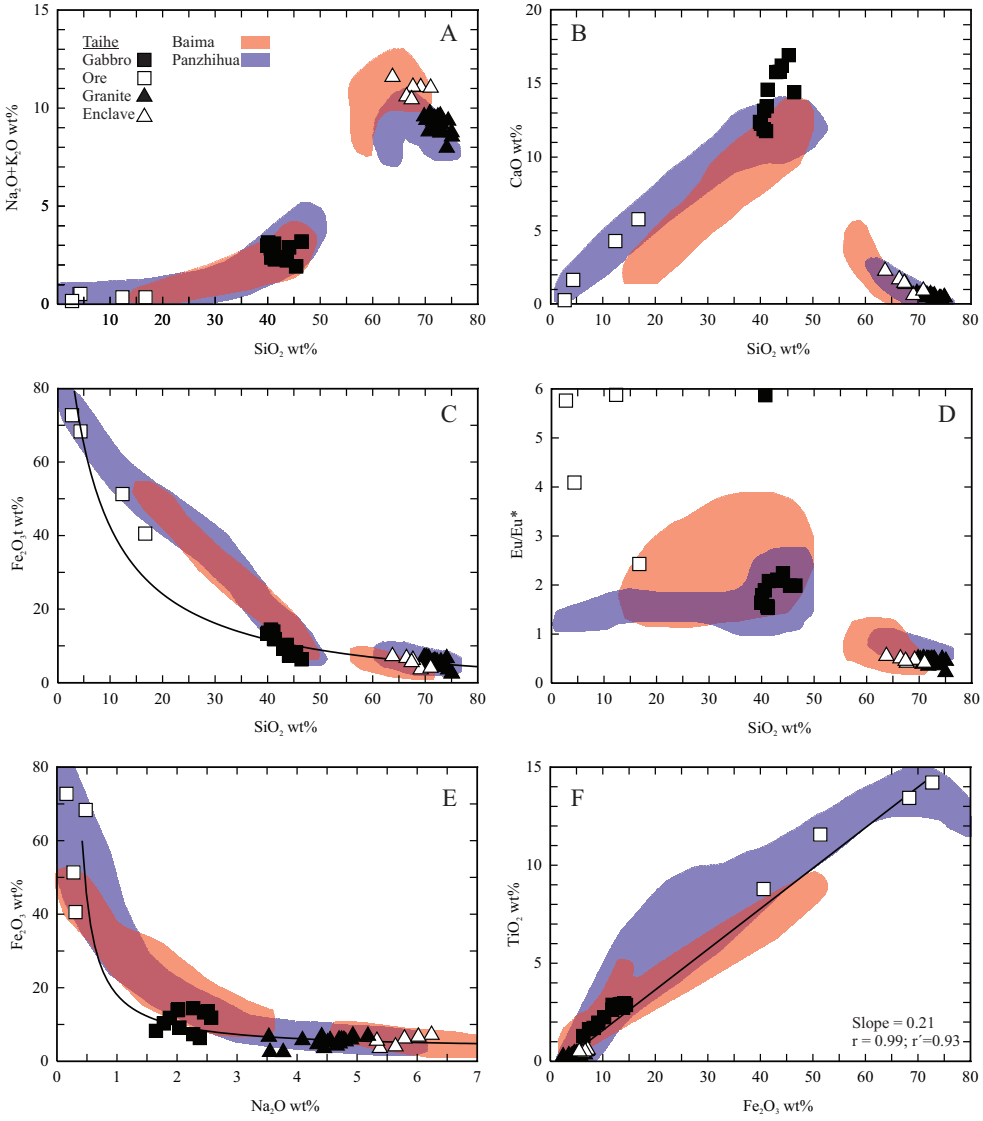

Fig. 5. Major element plots of the Taihe gabbros, granites and enclaves. Shown for reference are the mafic, intermediate and felsic rocks of the Baima and Panzhihua complexes (data from Shellnutt and Zhou, 2007; Shellnutt and others, 2009a, 2010; Shellnutt and Jahn, 2010).

COGENETIC LINK BETWEEN THE GABBROIC AND GRANITIC ROCKS

The 264 ± 3 Ma zircon U-Pb LA-ICP-MS age of the Taihe gabbro is similar to other plutonic and hypabyssal rocks of the ELIP (Zhou and others, 2005; Shellnutt and Zhou, 2007; Shellnutt and others, 2008, 2009a, 2011a; Xu and others, 2008; Zhong and others, 2011). The age of the gabbro obtained in this studied is within error of the neighboring Taihe (261 ± 2 Ma) peralkaline granite and the age (259 ± 2 Ma) reported by Zhong and others (2011). High precision zircon U-Pb TIMS dates of other granitic and mafic rocks of the Panxi region suggest the main period of magmatism was at ~260 Ma and probably did not extend beyond ~257 Ma (Shellnutt and others,

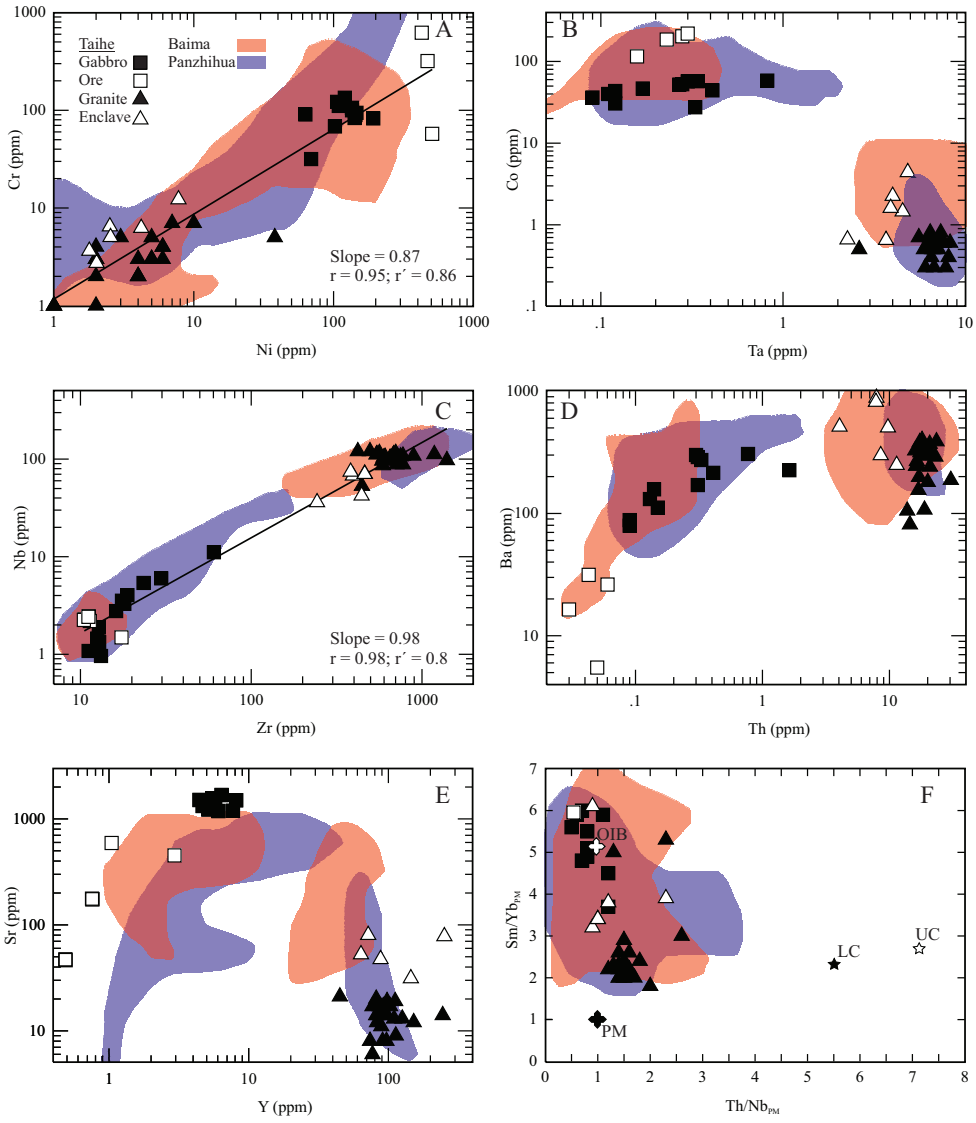

Fig. 6. Trace element plots of the Taihe gabbros, granites and enclaves. Shown for reference are the mafic, intermediate and felsic rocks of the Baima and Panzhihua complexes (data from Shellnutt and Zhou, 2007; Shellnutt and others, 2009a, 2010, Shellnutt and Jahn, 2010). PM = Primitive mantle and OIB = ocean-island basalt from Sun and McDonough (1989) and UC = upper crust and LC = lower crust from Rudnick and Gao (2003).

2011a). The Taihe gabbro is the third example of a spatially and temporally associated, Fe-Ti-oxide bearing layered gabbro intrusion and a peralkaline granitic pluton in the Panxi region and implies that a common or identical process is responsible.

Some major element trends show a compositional evolution from the cumulate gabbros to the granites. However, there is a distinct SiO_2 gap between the gabbro and the most primitive enclave composition (fig. 5), which ranges from ~46.5 weight percent to ~63 weight percent. The compositional gap may be related to the

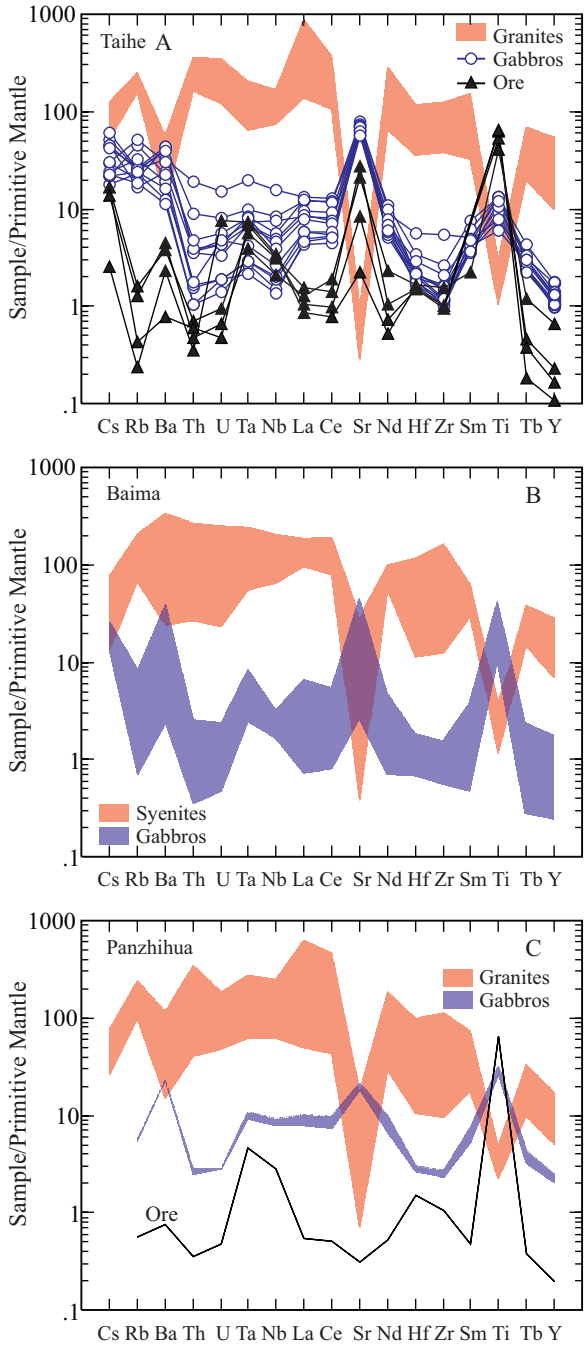

Fig. 7. Primitive mantle-normalized trace element plots of granitic and gabbroic rocks of the (A) Taihe complex, (B) Baima complex and (C) Panzhihua complex. Trace elements normalized to values of Sun and McDonough (1989). Additional data from Shellnutt and Zhou (2007), Shellnutt and others (2009a, 2010) and Shellnutt and Jahn (2010).

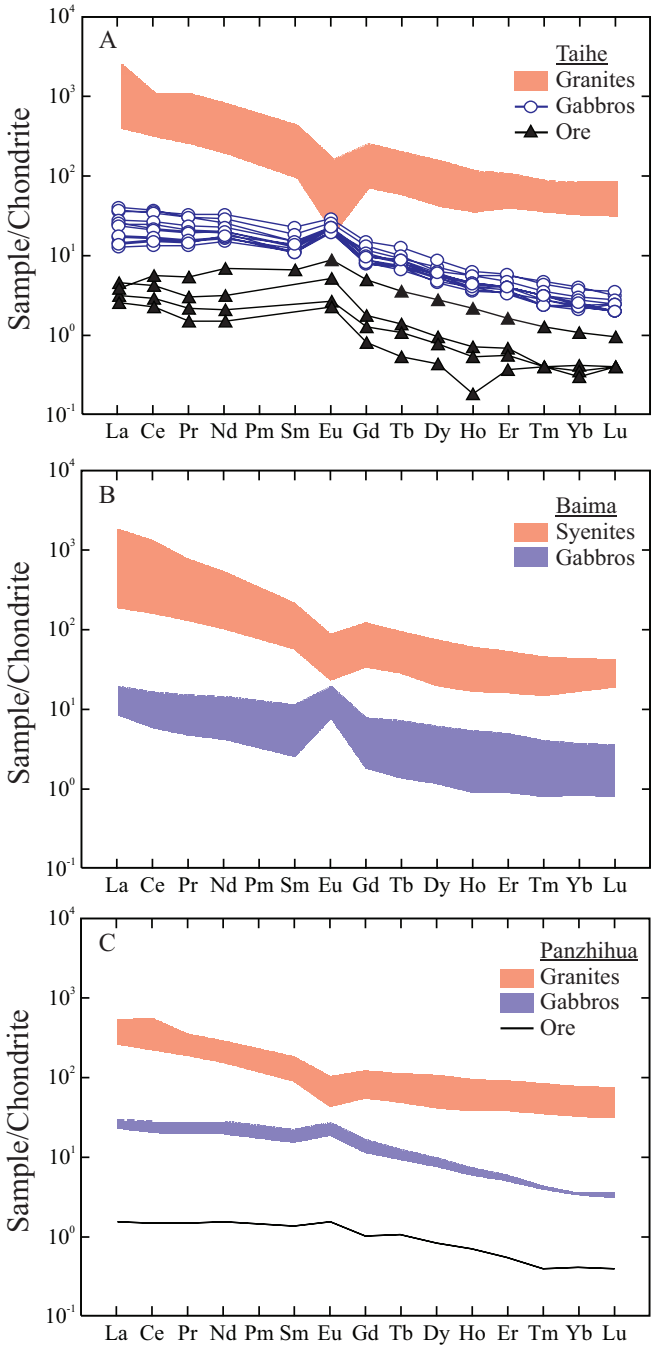

Fig. 8. Chondrite-normalized trace element plots of granitic and gabbroic rocks of the (A) Taihe complex, (B) Baima complex and (C) Panzhihua complex. Trace elements normalized to values of Sun and McDonough (1989). Additional data from Shellnutt and Zhou (2007), Shellnutt and others (2009a, 2010) and Shellnutt and Jahn (2010).

formation of the Fe-Ti oxide ore deposit (Shellnutt and others, 2009a; Natali and others, 2011).

The primitive mantle-normalized incompatible element patterns of the gabbros and felsic rocks are antithetical (fig. 7A). Uranium to Ce and Nd to Sm show low abundances in the gabbro and high in the granites, whereas Ba, Ti and Sr are enriched in the gabbro, and depleted in the granites. The chrondrite-normalized REE patterns also show the same relationship with respect to the Eu-anomalies (fig. 8A). The reciprocal Eu-anomalies in the gabbros and granites likely reflect the accumulation and fractionation of plagioclase. The low Sr (≤80 ppm) and Eu/Eu* (Eu/Eu* = 0.2 to 0.6) values of the granites and enclaves indicate that a significant amount of plagioclase fractionated from the parental magma.

The $\varepsilon Nd_{(T)}$ isotopic values ($\varepsilon Nd_{(T)}$ = +2.5 to +3.3) of the Taihe gabbros are slightly higher than the whole-rock $\varepsilon Nd_{(T)}$ values of the granites and enclaves of the Taihe pluton ($\varepsilon Nd_{(T)}$ = +1.0 to +2.0) but some are within the expected error range (for example, $\varepsilon Nd_{(T)} \pm 0.5$) suggesting that they may have originated from a similar mantle source and possibly the same parental magma (Shellnutt and Zhou, 2007; Shellnutt and others, 2009b, 2010). The zircon $\varepsilon Hf_{(T)}$ values of the gabbro ($\varepsilon Hf_{(T)}$ = 8.1 ± 0.8) are indistinguishable from those of the granites ($\varepsilon Hf_{(T)}$ = 9.2 ± 1.0) and provide support of a cogenetic relationship (Xu and others, 2008; Shellnutt and others, 2009b; Zhong and others, 2011, fig. 9). The slightly lower $\varepsilon Nd_{(T)}$ isotopic values from the granitic rocks suggest that there may have been some crustal assimilation within the magma system. The isotopic data fall along the mantle array and indicate that the magma source was likely derived from mixing between depleted mantle and at least one other component to produce a "mixed" isotopic signature. It is not certain whether the other component is, for example, crustal contamination or whether a subducted component (for example, GLOSS) within the source (for example, OIB-like source) is the explanation of the isotopic data (Chauvel and others, 2008). Some trace element ratios (for example, Th/Nb_{PM} and Nb/U), are sensitive to crustal assimilation and do not indicate that the crust was a major contributor to either the gabbros or granites (Th/Nb_{PM} of the crust = 6.9 crust; Th/Nb_{PM} = of the Taihe rocks < 3; Nb/U_{crust} = 9.7; average $Nb/U_{gabbros}$ = 33.9; average $Nb/U_{enclaves}$ = 34; average $Nb/U_{granites}$ = 24.6) (Campbell, 2002). Therefore we suggest that the zircon $\varepsilon Hf_{(T)}$ values and the higher $\varepsilon Nd_{(T)}$ values (for example, $\varepsilon Nd_{(T)} > +1.5$) are probably indicative of the mantle source composition of the parental magma (see fig. 6F).

GEOCHEMICAL MODELING

Shellnutt and others (2009a) and Shellnutt and Jahn (2010) have shown previously that the Baima and Panzhihua cumulate, Fe-Ti oxide-bearing gabbroic intrusions and silica-saturated peralkaline granitoids were likely formed by fractional crystallization of a common parental magma, which resembles high-Ti Emeishan flood basalts. The textural and compositional similarity of the Taihe gabbros and granites with the rocks of Baima and Panzhihua complexes suggests that the fractionation model may also be applicable. We test this hypothesis below.

Major Element Mass Balance

The compositions of olivine, clinopyroxene, plagioclase, magnetite and ilmenite from the Taihe gabbro (GS04-174) are used to determine if the composition of the Taihe granitic rocks can be reproduced from a parental magma equal to Emeishan basalt. The compositions of spinel (pleonaste) and apatite from the Panzhihua layered gabbro are used as proxies for these minerals in the Taihe gabbro (Pang and others, 2008a, 2008b, 2009). Since there are no known chilled margin compositions available, we use a parental magma composition, similar to sample SE-21 of Song and others

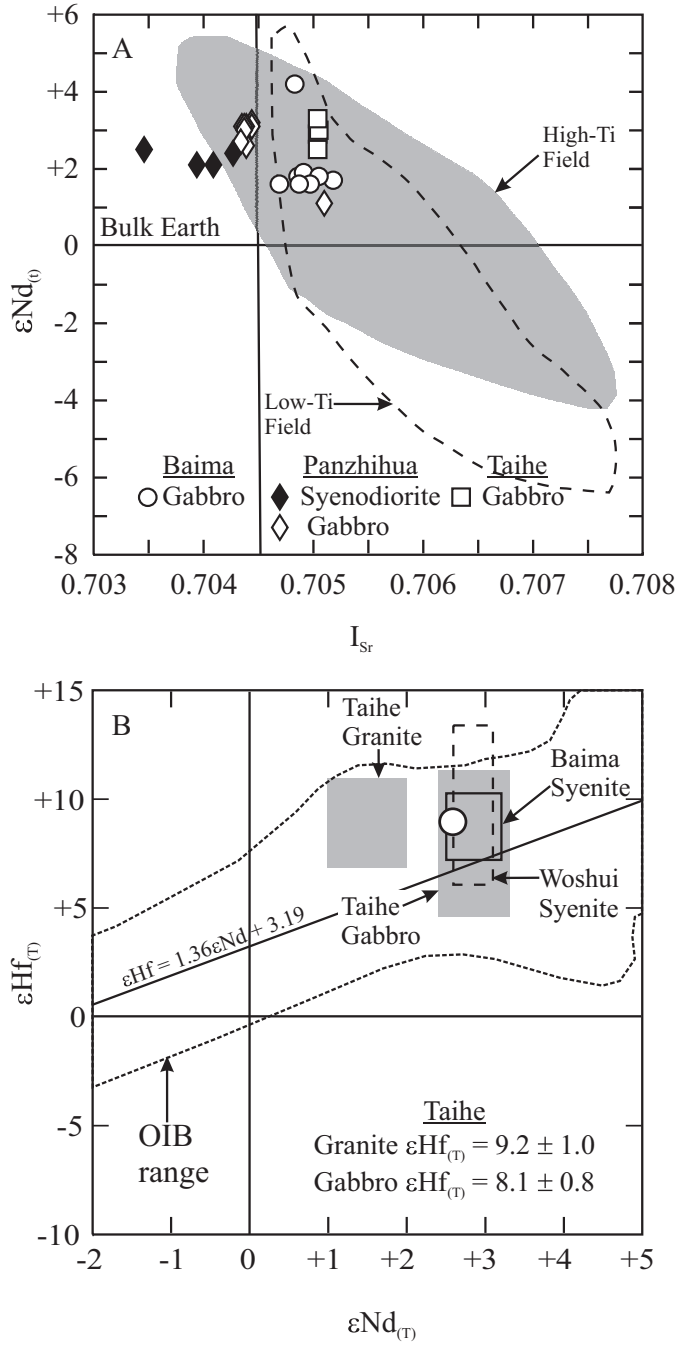

Fig. 9. (A) Whole-rock Sr-Nd radiogenic isotope results from the Taihe, Baima and Panzhihua complexes (Shellnutt and Zhou, 2007; Shellnutt and others, 2009a, 2010; Zhang and others, 2009; Shellnutt and Jahn, 2010). The isotopic data of the Emeishan basalts compiled from Xu and others (2001), Xiao and others (2003, 2004), Song and others (2004, 2008), Wang and others (2007), Fan and others (2008), Qi and others (2008), Qi and Zhou (2008), Shellnutt and others (2008). (B) Zircon $\varepsilon Hf_{(T)}$ values versus whole-rock $\varepsilon Nd_{(T)}$ values from the Taihe gabbro and granites and the Baima syenites and metaluminous Woshui syenite. The white circle is data reported by Zhong and others (2011) for the Taihe gabbro. The $\varepsilon Nd_{(T)}$-$\varepsilon Hf_{(T)}$ field for ocean-island basalts from Vervoort and Blichert-Toft (1999) and Kempton and others (2000). Additional data from Shellnutt and Zhou (2007) and Shellnutt and others (2009a, 2009b).

(2001), to calculate the proportion of cumulate minerals required to produce the granite composition.

Table 9 shows the results of the mass balance calculations. If 8.5 percent olivine (Fo_{76}), 28.2 percent clinopyroxene ($Wo_{49}En_{41}Fs_{10}$), 21.5 percent plagioclase (An_{70}), 3.8 percent ilmenite, 5.6 percent magnetite, 0.7 percent apatite and 0.1 percent spinel in mass units totaling ~68 percent of the starting composition are removed from the assumed parental magma composition, then the residual composition is very similar to the average composition of the Taihe granites (table 9). The modeled modal values of the cumulate minerals are similar to the bulk content reported by Yao and others (1993). This method is semi-quantitative because the crystallizing minerals would not have constant compositions. The results do not provide definitive evidence for a comagmatic origin but suggest that the Taihe layered gabbroic unit could represent ~68 percent of the total parental magma composition.

MELTS Modeling

The thermodynamic evolution of the mafic and felsic rocks can be modeled using the program MELTS (Ghiorso and Sack, 1995; Smith and Asimow, 2005). We take a similar parental magma composition (that is sample SE-21 with K_2O = 1.4 wt% instead of 1.0 wt%) for the mass balance calculations and apply MELTS. With conditions of fO_2 = FMQ − 1, starting temperature of 1300 °C, H_2O = 0.50 weight percent, and pressure of 600 bars (~2 km) we demonstrate that reasonable estimates of the observed rock compositions can be generated.

Figure 10 compares the results from the MELTS model with the observed data of the enclaves and granites normalized to 100 percent. The enclave compositions are not interpreted to represent liquid compositions, and therefore they are not expected to fall along the model trend lines (Shellnutt and others, 2010). The Taihe granitic compositions can be modeled with respect to Al_2O_3, TiO_2, FeOt, Na_2O+K_2O and MgO, whereas CaO and P_2O_5 are somewhat problematic as the model curves tend to be too high. The problems with Ca and P are likely due to a combination of apatite, fluorite, titanite and Ce-monazite crystallization (Shellnutt and Iizuka, 2011). These minerals are present within the granite, albeit in low quantities. However, MELTS cannot model the fractionation of fluorite and monazite, and thus it is a possible explanation for the discrepancy between the observed data and the modeled trends. Furthermore, the crystallization of fluorite can promote alkali enrichment within a felsic magma and therefore the modeled compositional evolution lines may be low (Bailey, D. K., 1974; Bailey, J. C., 1977; Harris and Marriner, 1980).

The model predicts early crystallization of olivine (Fo_{81}) at 1200 °C followed by clinopyroxene ($Wo_{44}En_{43}Fs_{13}$) at 1145 °C and plagioclase (An_{65}) at 1105 °C. The crystallization of Fe-rich spinel (that is magnetite series spinel) begins when the temperature reaches ~1090 °C and represents one third of the total mineral assemblage crystallizing at that point. As the temperature drops to 1055 °C, ~63 percent of total oxides that will crystallize in the entire system have formed and the residual liquid SiO_2 content in the model increases rapidly from 53.0 weight percent to 60.0 weight percent. The proportion of spinel crystallizing drops continuously until 870 °C, at which point it no longer crystallizes. The residual liquid composition continues to evolve and reaches compositions similar to the most primitive enclave as the temperature drops to 1005 °C is followed by granitic compositions between 935 °C to 885 °C.

Trace Element Modeling

Selected trace elements were used to model the possible chemical evolution of the Taihe gabbro-granite complex. Barium, Sr, Ni, Co, Nb and Ta were chosen because they are primarily controlled by major minerals (for example plagioclase, alkali feldspar, olivine, titanite) within each rock type and their partition coefficients are

TABLE 9

Mass-balance calculation for the Taihe gabbro-granite complex

Sample	SiO_2	TiO_2	Al_2O_3	FeOt	MnO	MgO	CaO	Na_2O	K_2O	P_2O_5	Total
Hi-Ti	50.20	2.60	12.30	12.10	0.20	7.40	9.90	2.60	1.40	0.30	99.00
Hi-Ti*	27.70	2.47	8.69	10.63	0.12	7.32	9.74	0.73	0.07	0.29	67.77
Remaining ^{Granite}	22.50	0.13	3.61	1.47	0.08	0.08	0.16	1.87	1.33	0.01	31.23
Normalized$^{1Hi\text{-}Ti*}$	40.88	3.65	12.83	15.68	0.18	10.80	14.37	1.08	0.10	0.43	100.00
Normalized^{2Granite}	72.03	0.41	11.55	4.71	0.24	0.26	0.51	5.99	4.27	0.02	100.00

Sample	SiO_2	TiO_2	Al_2O_3	FeOt	MnO	MgO	CaO	Na_2O	K_2O	P_2O_5	Total
Granite Average	72.27	0.39	11.10	4.73	0.14	0.13	0.55	4.50	4.65	0.02	98.46

Mineral	Olivine	Cpx	Plagioclase	Plagioclase	Ilmenite	Magnetite	Apatite	Spinel
	Fo75		An83	An70				
Element								
SiO_2	39.62	48.88	48.49	49.06	0.00	0.00	0.08	0.00
TiO_2	0.04	1.89	0.06	0.06	50.99	0.19	0.00	0.11
Al_2O_3	0.01	5.96	33.20	32.18	0.02	0.52	0.00	62.20
FeOt	22.28	6.03	0.30	0.35	47.37	91.89	1.80	23.63
MnO	0.24	0.17	0.00	0.00	1.47	0.00	0.10	0.17
MgO	39.38	14.01	0.01	0.03	0.03	0.00	0.00	13.22
CaO	0.03	23.06	16.69	13.35	0.03	0.05	52.00	0.00
Na_2O	0.08	0.34	1.88	2.92	0.01	0.00	0.00	0.08
K_2O	0.00	0.01	0.03	0.29	0.00	0.00	0.00	0.00
P_2O_5	0.00	0.00	0.00	0.00	0.00	0.00	42.00	0.00

	ol%	cpx %	pl83 %	pl70%	il %	mt %	ap%	sp%	Total
Hi-Ti*	8.5	28.2	0	21.5	3.8	5.6	0.7	0.1	68.4

Mineral symbols: Fo = forsterite component; An = anorthite component; ol = olivine; cpx = clinopyroxene; pl = plagioclase; il = ilmenite; mt = magnetite; ap = apatite; sp = spinel.

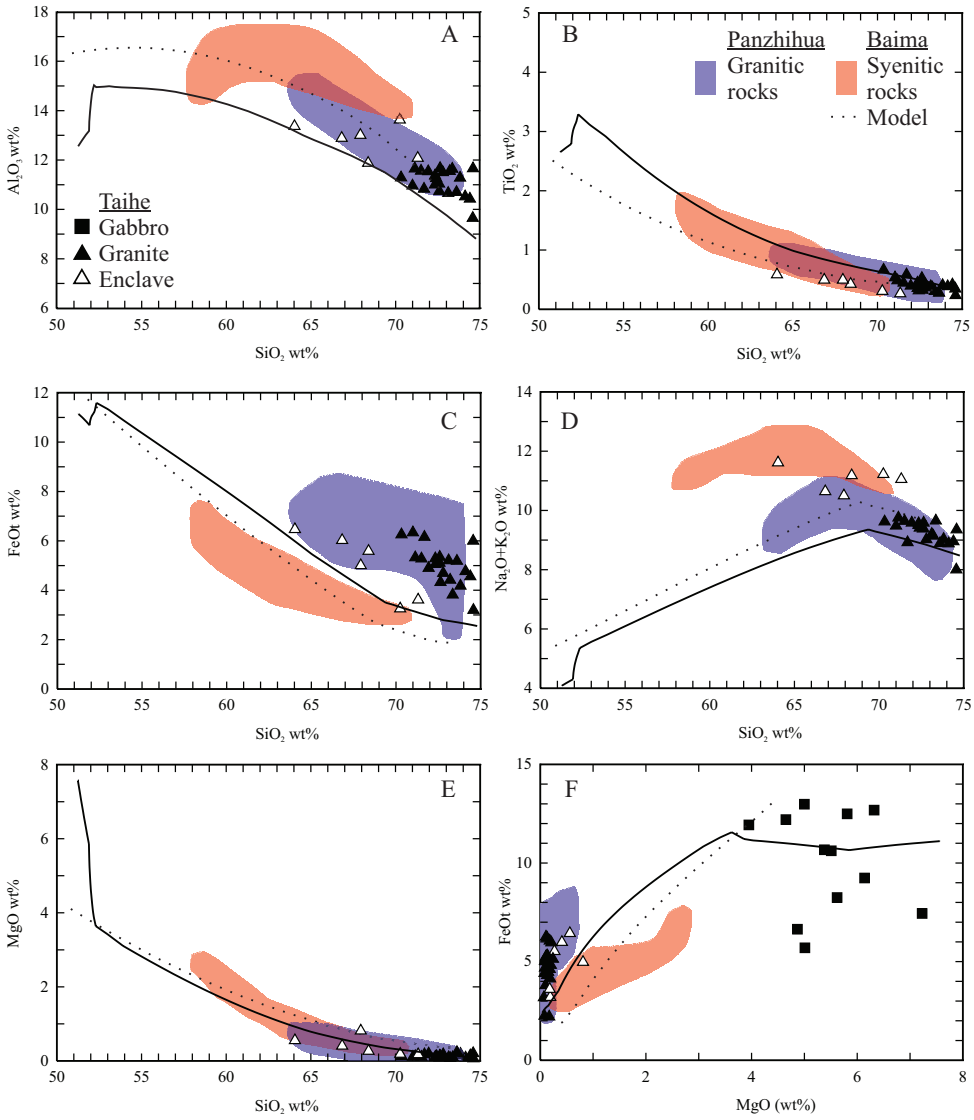

Fig. 10. Results from MELTS modeling showing the liquid compositional evolution curve for the Taihe granites and enclaves (solid line). The dotted line represents the evolution curve for the Baima enclaves and syenites. The solid line may also be appropriate for the Panzhihua granites and syenodiorites. Additional data from Shellnutt and Zhou (2007), Shellnutt and others (2009a, 2010) and Shellnutt and Jahn (2010).

reasonably well constrained. Since the parental magma trace element composition is unknown, we chose values that are representative of Emeishan "high-Ti" basalts and sample SE-21. We assumed a starting composition with Ba = 475 ppm; Sr = 550 ppm; Ni = 115 ppm; Co = 54 ppm, Nb = 24 ppm; Ta = 1.6 ppm. We subdivided the Taihe layered gabbro into four groups, which are similar to the subgroups described by Yao and others (1993) although we treat the ores as a separate group. The lower group is the most primitive group and contains the most olivine (25% olivine, 40% clinopyroxene, 20% plagioclase, 15% magnetite). The ore group is assumed to represent the bulk

of the oxide deposit and consists mostly of magnetite (5% olivine, 5% clinopyroxene, 5% plagioclase, 85% magnetite). The two remaining groups are gabbroic in composition. However they have more plagioclase and clinopyroxene and less olivine than the lower group (Middle group = 5% olivine, 25% clinopyroxene, 65% plagioclase, 5% magnetite; Upper group = 20% clinopyroxene, 80% plagioclase). Based on the above subdivisions, the bulk mineral content (olivine = 11%, clinopyroxene = 26%, plagioclase = 46%, magnetite = 18%) are similar to the mineral modes described by Yao and others (1993) and Zhong and others (2011).

We calculated the bulk partition coefficients of Ba, Sr, Ni, Co, Nb and Ta using the mineral modes for each group and published mineral/melt partition coefficients (table 10). The modeling results can reproduce the observed compositional trends form the parental mafic magma to the enclaves and granites. Figure 11A shows the melt evolution path of Ba and Sr. The fractionation of the lower group and ore assemblages (oxide-rich assemblages) increase the amount of Ba and Sr in the melt, whereas the fractionation of the middle and upper groups (silicate-rich assemblages) show enrichment of Ba and depletion of Sr. As the most primitive enclave compositions are reached, Ni and Co become depleted (fig. 11B) and Nb and Ta and become enriched (fig. 11B). When Ni and Co are nearly exhausted, the melt composition is similar to the observed enclave composition at ~72 percent crystallization. Because Ni and Co are almost exhausted and compositions similar to the enclaves are reached, the fractionating mineral assemblage must change to reflect the new bulk composition. Fractionation of alkali feldspar with quartz, amphibole and a minor amount of titanite can explain the trend from 28 percent to 0 percent liquid (fig. 11).

A TRIUMVIRATE OF GABBRO-GRANITE COMPLEXES

The presence of at least three, independent, gabbro-granitoid complexes within ~200 km of each other is a rare phenomenon. It suggests that the formation of this type of magmatic system was common within the Panxi area and possibly the entire ELIP. Previous studies on the Baima and Panzhihua complexes described a model of shallow level (that is ~1 kbar) fractionation of "high-Ti" basalt (Shellnutt and others, 2009a; Shellnutt and Jahn, 2010). The basalt distinction is important because the "high- and low-Ti" Emeishan flood basalts reflect the propensity for certain types of metal deposits (high-Ti basalt = Fe-Ti deposits; low-Ti = sulphide deposits; Wang and others, 2007; Zhou and others, 2008).

In all three cases, the geochemical evidence indicates that there is a genetic link between the layered gabbroic intrusion and the spatially and temporally associated intermediate and felsic rocks. Trace element pairs, reciprocal primitive mantle-normalized incompatible element patterns and reciprocal Eu/Eu* values indicate the accumulation of olivine, plagioclase, clinopyroxene and magnetite, which could generate residual liquids depleted in Ni, Co, Sc, Cr, Ti, Ba, Sr and Eu and enriched in Rb, Th, U, Nb, Ta, REEs (except Eu), Zr, Hf, Y.

It is inferred from the $\varepsilon Nd_{(T)}$, zircon $\varepsilon Hf_{(T)}$, and I_{Sr} values that the magma source characteristics of the gabbro-granitoid complexes are very similar. The $\varepsilon Nd_{(T)}$ values of clinopyroxenes ($\varepsilon Nd_{(T)}$ = +1.1 to +3.2) from the Panzhihua gabbros overlap with the whole-rock $\varepsilon Nd_{(T)}$ values of the Baima ($\varepsilon Nd_{(T)}$ = +1.6 to +4.2) and Taihe gabbros ($\varepsilon Nd_{(T)}$ = +2.5 to +3.3) and granitoids (Panzhihua $\varepsilon Nd_{(T)}$ = +2.2 to +2.9; Baima $\varepsilon Nd_{(T)}$ = +2.5 to +3.2; Taihe $\varepsilon Nd_{(T)}$ = +1.0 to +2.0) suggesting that they originated from the same source (fig. 9A; Shellnutt and others, 2009a, 2010; Zhang and others, 2009). The available zircon $\varepsilon Hf_{(T)}$ values from the Baima syenite ($\varepsilon Hf_{(T)} = 8.7 \pm 0.4$), Taihe granite $\varepsilon Hf_{(T)} = 9.2 \pm 1.0$) and gabbro ($\varepsilon Hf_{(T)} = 8.1 \pm 0.8$) and the temporally related Woshui syenite ($\varepsilon Hf_{(T)} = 8.6 \pm 0.2$) are within the same range (fig. 9B; Shellnutt and others, 2009b; Zhong and others, 2011). The I_{Sr} values of the peralkaline rocks are a little more difficult to interpret because they are very low (<0.700), which

TABLE 10

Partition coefficients (D) of the Taihe gabbroic zones and granites

Zone	Lower		Ore		Middle		Upper		kD				Granite	kD			
Element	Literature Value	Bulk D	Literature Value	Bulk D	Literature Value	Bulk D	Literature Value	Bulk D	ol	px	pl	mt	Bulk D	alk	tn	amp	qz
Sr	0.62	0.59	0.15	0.14	1.91	2.56	2.34	3.97	0.014	0.10	2.9		3.55	4.3		3.0	
Ba	0.21	0.19	0.05	0.05	0.65	0.60	0.80	0.76	0.030	0.001	1.0		3.16	4.3		0.39	0.022
Ni	3.71	9.15	6.44	11.58	1.14	1.18	0.30	0.26	8.25	1.5		7	1.24	1.32		2	
Co	3.56	7.67	6.72	12.84	1.20	1.26	0.40	0.35	6.6	2.0		7.4	1.37	0.39		7.26	
Nb	0.20	0.18	1.11	1.11	0.07	0.06	0.01	0.01	0.01	0.005	0.01	1.3	0.42	0.1	7.6	0.8	
Ta	0.02	0.02	0.09	0.08	0.01	0.01				0.013		0.1	0.63	0.01	16.5	0.85	0.008

Lower = lower cumulate zone, Ore = oxide ore zone, Middle = olivine gabbro zone, Upper = upper gabbro zone. Percentages of olivine (ol), plagioclase (pl), clinipyroxene (px), and magnetite (mt) for the Lower = 25% ol, 20% pl, 40% px, 15% mt; Ore = 5% ol, 5% pl, 5% px, 85% mt; Middle = 5% ol, 65% pl, 25% px, 5% mt; Upper = 0% ol, 80% pl, 20% px, 0% mt. Percentages of alkali feldspar (alk), titanite (tn), amphibole (amp), and quartz (qz) for the granite = 72% alk, 3% tn, 15% amp, 10% qz. Mineral melt partition coefficients taken from Leeman and Scheidegger (1977), Matsui and others (1977), Villemant and others (1981), Mahood and Hildreth (1983), Green and Pearson (1987), Nielsen (1992), Hart and Dunn (1993), Rollinson (1993), Ewart and Griffin (1994), Hauri and others (1994), and Marks and others (2004). Literature value is the calculated bulk distribution coefficient using published partition coefficients and mineral modes. The Bulk D value is the value calculated from the fractionation model.

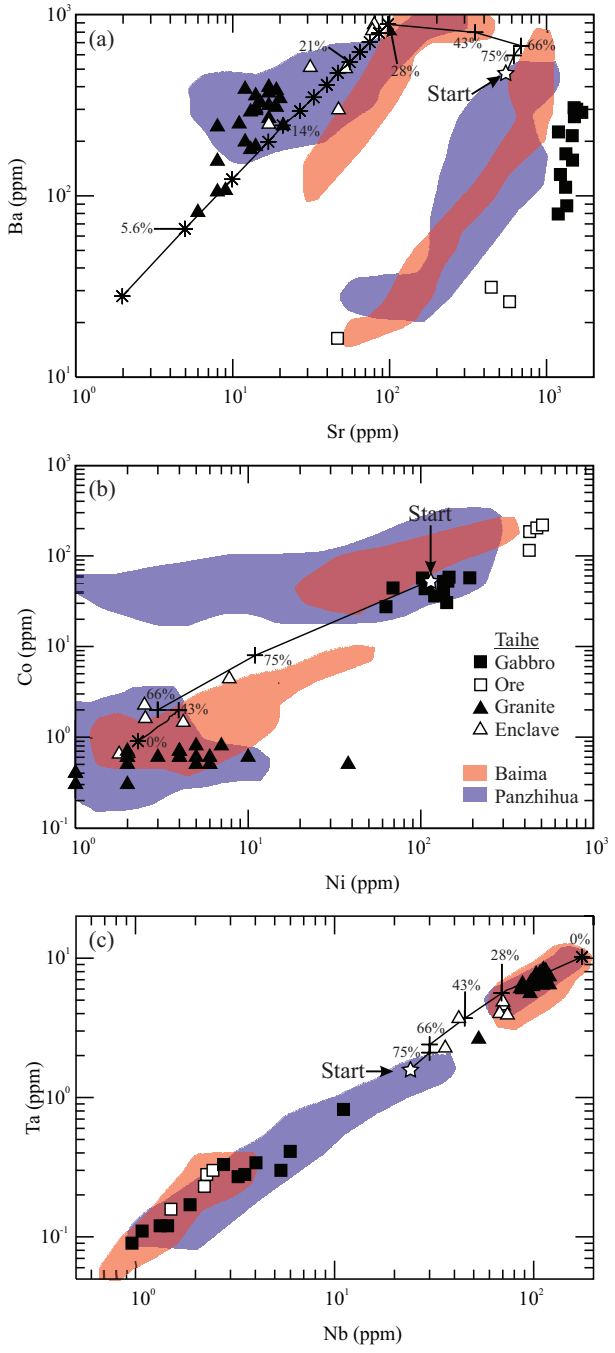

Fig. 11. Results of trace element modeling of the Taihe parental magma: (A) Ba (ppm) versus Sr (ppm), (B) Co (ppm) versus Ni (ppm), and (C) Ta (ppm) versus Nb (ppm). The starting (star) composition is assumed to have Sr = 550 ppm, Ba = 475 ppm, Nb = 24 ppm, Ta = 1.6 ppm, Ni = 115 ppm and Co = 54 ppm. The residual liquid composition (*) is shown evolving at the melt fraction percentages using the bulk partition coefficients of the Lower, Ore, Middle and Upper zones until reaching 28%.

may be due to Sr loss and Rb gain by deuteric alteration. However, the I_{Sr} values of the Panzhihua gabbro (I_{Sr} = 0.70434 to 0.70510) and syenodiorite (I_{Sr} = 0.70346 to 0.70427), Baima gabbro (I_{Sr} = 0.70469 to 0.70518) and Taihe gabbro (I_{Sr} = 0.70504 to 0.70505) are similar.

The mineral and whole-rock compositions of the Panzhihua and Taihe granites are very similar but differ from those of the Baima syenites (Shellnutt and Iizuka, 2011). The same may be true for the layered gabbroic rocks. Overall, the Baima gabbro appears to contain more olivine and has higher bulk MgO when compared to the gabbroic rocks of the Panzhihua and Taihe complexes. The mineralogy of the granitic rocks indicates that the relative oxidation states of the granitic plutons was likely different. The Baima syenites contain quartz, titanite, magnetite and Mg-rich ferrorichterite, which indicates fO_2 = FMQ $\geq$ 0 (Wones, 1989). In comparison, the Panzhihua and Taihe granites contain Fe-rich ferrorichterite and aenigmatite, which are indicative of reducing conditions (fO_2 = FMQ $<$ 0). The MELTS modeling results for the three gabbro-granitoid complexes is consistent with the granitoid mineralogy in the sense that the Baima model has the best results with fO_2 = FMQ $\geq$ 0 and the Panzhihua and Taihe models with fO_2 = FMQ − 1. In addition to the magma oxidation state, it is likely that the parental magmas were different as well (table 2). The parental magma of the Baima complex is assumed to be similar to sample EM-81 of Xu and others (2001), whereas the parental magmas of the Panzhihua and Taihe complexes are thought to be similar to GS03-003 and SE-21 (Song and others, 2001; Shellnutt and others, 2009a; Shellnutt and Jahn, 2010). Sample EM-81 has lower SiO_2 (~44.5 wt%), MgO (6.9 wt%), total alkalies (~3.5 wt%) and higher TiO_2 (~3.5 wt%), Fe_2O_3t (~16.4 wt%), Al_2O_3 (13.8 wt%) and CaO (~10.15 wt%) than SE-21 and GS01-003 (table 2). The combination of the relative magmatic oxidation state and the parental composition are the likely reasons why the Baima complex formed syenites rather than granites.

The relative emplacement depth is difficult to estimate for the Baima and Taihe plutons because the geological relationships do not indicate how close to the surface they intruded. In contrast to the Baima and Taihe complexes, the Panzhihua granitic pluton intruded subaerial Emeishan basalts and likely served as a magma reservoir for compositionally similar trachytes indicating a shallow emplacement depth (Shellnutt and Jahn, 2010). Based on the geological relationships of the Panzhihua granite, the inferred depth of emplacement for the other complexes is also likely to be shallow (≤1 kbar) (Pang and others, 2010).

The MELTS temperature range for the peralkaline plutons are within the expected temperature range of some A-type granitic rocks (870 °C to 950 °C) and the results of zirconium saturation thermometry (T_{Zr}(°C)) estimates (Clemens and others, 1986; Creaser and others, 1991; White and others, 2005; Shellnutt and Iizuka, 2011). The Baima syenites have a slightly lower average T_{Zr}(°C) of ~860 ± 17 °C when compared to the MELTS results (T°C = 880 °C to 970 °C) but the MELTS temperature ranges (T°C = 885 °C to 935 °C) for the Panzhihua and Taihe granites are very similar to the T_{Zr}(°C) calculations (Panzhihua T_{Zr}(°C) = 940 °C ± 21; Taihe T_{Zr}(°C) = 897 °C ± 14) and match the range estimated by Pang and others (2008a, 2008b) for the end of oxide-silicate equilibration in the Panzhihua layered mafic intrusion (~950 °C).

DIFFERENCES WITH OTHER OXIDE DEPOSITS

There are many layered gabbroic intrusions throughout the world that host orthomagmatic Cr- and Fe-Ti-V oxide deposits (Lee, 1996). Oxide-bearing gabbroic intrusions are often associated spatially and temporally with granitic rocks, but this does not necessarily imply that they are coherent igneous complexes (Weibe, 1996; Bonin, 2007). The Bushveld (South Africa), Suwalki (Poland), Smålands Taberg

(Sweden), Stillwater (USA), Muskox (Canada) and Kiglapait (Canada) intrusions are only a few of the cumulate-rich layered mafic-ultramafic complexes which have Cr-rich or Fe-Ti-rich oxide minerals (Morse, 1969; Irvine, 1977; Speczik and others, 1988; Eales and Cawthorn, 1996; McCallum, 1996; Sandecki, 2000). If present, the Fe-Ti oxide-rich layers tend to be located in the upper parts of their host intrusions and the petrogenetic link of these intrusions either temporally or spatially associated A-type granitic rocks remains to be confirmed (Bonin, 2007; Pang and others, 2010). Furthermore, some of the intrusions show evidence of being dynamic open magma systems (for example, the Bushveld Complex) and/or were emplaced at greater depths (for example, Stillwater) than those for the Panxi complexes.

In comparison to other oxide-bearing layered intrusions, the Panxi gabbro-granitoid complexes contain only Fe-Ti oxide deposits in their lower portions and appear to be formed by relatively closed systems (Shellnutt and others, 2009a; Shellnutt and Jahn, 2010). It is not clear if this style of deposit is unique to the Panxi region or if it also exists in other places due to the fact that gabbroic and granitic intrusions are often examined separately in spite of their spatial associations. Given that crystal fractionation is a universal process, it stands to reason that similar magmatic conditions as the Panxi gabbro-granitoid-oxide complexes may be met everywhere, but that does not necessarily mean that such complexes will always form. The magmatic conditions that generated the "Panxi-style" deposits include: shallow emplacement levels ($\leq$3 km), OIB-like, Fe-rich parental magmas, fO_2 = FMQ $\pm$ 1, sufficient time to differentiate and limited country rock interactions. Price and others (1999) have suggested similar conditions for the formation of some A-type granites (for example, high-temperature conditions, shallow-crystallization environments, moderate fO_2). The ideal environment for such conditions is an extensional, within-plate setting (Eby, 1990).

IMPLICATIONS OF THE GABBRO-GRANITIC COMPLEXES

The important implications from the work compiled from the Panxi gabbro-granitoid complexes are: 1) some peralkaline, silica-saturated, A-type granitoids are derived by shallow level fractional crystallization of mafic magmas under oxidizing or reducing conditions, 2) the formation of "Panxi-type" massive oxide deposits do not appear to require assimilation of crustal material or magmatic fluids to enrich the evolving liquid in metals, 3) "Panxi-type" deposits may be common within continental LIPs provided OIB-like lavas are present and 4) silica saturated peralkaline granitic rocks may be used as indicators for magmatic Fe-Ti oxide deposits.

CONCLUSIONS

The Taihe layered gabbroic intrusion is one of at least three gabbro-granitoid-oxide complexes within the Panxi region of the Emeishan large igneous province. The major and trace elemental data, Sr-Nd isotopic data and zircon Hf isotopic data suggest that the gabbros and granites are genetically related. Mass-balance and geochemical modeling indicate that it is possible to derive the granites by fractional crystallization of a parental magma resembling Emeishan "high-Ti" basalt. MELTS modeling suggests the parental magmatic conditions for the Taihe gabbro-granite complex are: ~0.6 kbar, $H_2O \cong 0.5$ weight percent and $fO_2 \cong$ FMQ $-$ 1. The shallow emplacement depth and lower fO_2 are consistent with the textures and mineralogy of the granites (for example, aenigmatite, Mn-rich ilmenite and perthitic alkali feldspar). The occurrence of at least three Fe-Ti oxide-bearing gabbro-granitoid complexes within the Panxi region suggests that the formation of similar complexes may be common within the Emeishan large igneous province and possibly other large igneous provinces which erupted OIB-like magmas.

ACKNOWLEDGMENTS

We would like to thank Eero Hanski and an anonymous reviewer for their constructive comments that helped to improve this manuscript. The authors would like to thank Professor Ma Yuxiao and Mr. Zhao Hao, both from Chengdu University of Science and Technology, for their field support, and Ms. Xiao Fu for her analytical support at the University of Hong Kong. We are grateful to HY Chiu and IJ Lin for their analytical support at National Taiwan University. JGS acknowledges the support from the National Science Council through grant NSC100-2116-M-003-006-MY2.

References

Ali, J. R., Thompson, G. M., Zhou, M.-F., and Song, X. Y., 2005, Emeishan large igneous province, SW China: Lithos, v. 79, n. 3–4, p. 475–489, http://dx.doi.org/10.1016/j.lithos.2004.09.013

Bailey, D. K., 1974, Experimental petrology relating to oversaturated peralkaline volcanics: a review: Bulletin of Volcanology, v. 38, n. 2, p. 637–652, http://dx.doi.org/10.1007/BF02596901

Bailey, J. C., 1977, Fluorine in granitic rocks and melts: A review: Chemical Geology, v. 19, n. 1–4, p. 1–42, http://dx.doi.org/10.1016/0009-2541(77)90002-X

Belousova, E. A., Griffin, W. L., O'Reilly, S. Y., and Fisher, N. I., 2002, Igneous zircon: trace-element composition as an indicator of source rock type: Contributions to Mineralogy and Petrology, v. 143, n. 5, p. 602–622, http://dx.doi.org/10.1007/s00410-002-0364-7

Bonin, B., 2007, A-type granites and related rocks: evolution of a concept, problems and prospects: Lithos, v. 97, n. 1–2, p. 1–29, http://dx.doi.org/10.1016/j.lithos.2006.12.007

Bouvier, A., Vervoort, J. D., and Patchett, P. J., 2008, The Lu-Hf and Sm-Nd isotopic composition of CHUR: Constraints from unequilibrated chondrites and implications for the bulk composition of terrestrial planets: Earth and Planetary Science Letters, v. 273, n. 1–2, p. 48–57, http://dx.doi.org/10.1016/j.epsl.2008.06.010

Bryan, S. E., and Ernst, R. E., 2008, Revised definition of Large Igneous Provinces (LIPs): Earth-Sciences Review, v. 86, n. 1–4, p. 175–202, http://dx.doi.org/10.1016/j.earscirev.2007.08.008

Campbell, I. H., 2002, Implications of Nb/U, Th/U and Sm/Nd in plume magmas for the relationship between continental and oceanic crust formation and the development of the depleted mantle: Geochimica et Cosmochimica Acta, v. 66, n. 9, p. 1651–1661, http://dx.doi.org/10.1016/S0016-7037(01)00856-0

Cawthorn, R. G., 1996, Layered Intrusions: Amsterdam, Elsevier, Developments in Petrology, v. 15, 531 p.

Chauvel, C., Lewin, E., Carpenter, M., Arndt, N. T., and Marini, J. C., 2008, Role of recycled oceanic basalt and sediment in generating the Hf-Nd mantle array: Nature Geosciences, v. 1, p. 64–67, http://dx.doi.org/10.1038/ngeo.2007.51

Chiu, H. Y., Chung, S.-L., Wu, F. Y., Liu, D., Liang, Y. H., Lin, I. J., Iizuka, Y., Xie, L. W., Wang, Y., and Chu, M. F., 2009, Zircon U-Pb and Hf isotopic constraints from eastern Transhimalayan batholiths on the precollisional magmatic and tectonic evolution in southern Tibet: Tectonophysics, v. 477, n. 1–2, p. 3–19, http://dx.doi.org/10.1016/j.tecto.2009.02.034

Chung, S.-L., and Jahn, B.-M., 1995, Plume-lithosphere interaction in generation of the Emeishan flood basalts at the Permian-Triassic boundary: Geology, v. 23, n. 10, p. 889–892, http://dx.doi.org/10.1130/0091-7613(1995)023⟨0889:PLIIGO⟩2.3.CO;2

Clemens, J. D., Holloway, J. R., and White, A. J. R., 1986, Origin of an A-type granite: experimental constraints: American Mineralogist, v. 71, p. 317–324.

Creaser, R. A., Price, R. C., and Wormald, R. J., 1991, A-type granites revisited: assessment of a residual-source model: Geology, v. 19, n. 2, p. 163–166, http://dx.doi.org/10.1130/0091-7613(1991)019⟨0163:ATGRAO⟩2.3.CO;2

De Bièvre, P., and Taylor, P. D. P., 1993, Table of the isotopic compositions of the elements: International Journal of Mass Spectrometry and Ion Processes, v. 123, n. 2, p. 149–166, http://dx.doi.org/10.1016/0168-1176(93)87009-H

Eales, H. V., and Cawthorn, R. G., 1996, The Bushveld Complex, *in* Cawthorn, R. G. editor, Layered Intrusions: Amsterdam, Elsevier, Developments in Petrology, v. 15, p. 181–232.

Eby, G. N., 1990, The A-type granitoids: a review of their occurrence and chemical characteristics and speculations on their petrogenesis: Lithos, v. 26, n. 1–2, p. 115–134, http://dx.doi.org/10.1016/0024-4937(90)90043-Z

Ewart, A., and Griffin, W. L., 1994, Application of Proton-Microprobe Data to Trace-Element Partitioning in Volcanic-Rocks: Chemical Geology, v. 117, n. 1–4, p. 251–284, http://dx.doi.org/10.1016/0009-2541(94)90131-7

Fan, W., Zhang, C., Wang, Y., Guo, F., and Peng, T., 2008. Geochronology and geochemistry of Permian basalts in western Guangxi Province, southwest China: evidence for plume-lithosphere interaction: Lithos, v. 102, n. 1–2, p. 218–236, http://dx.doi.org/10.1016/j.lithos.2007.09.019

Ferreira, V. P., Sial, A. N., and Whitney, J. A., 1994, Large-scale silicate liquid immiscibility: a possible example from northeastern Brazil: Lithos, v. 33, n. 4, p. 285–302, http://dx.doi.org/10.1016/0024-4937(94)90034-5

Ganino, C., and Arndt, N. T., 2009, Climate changes caused by degassing of sediments during the emplacement of large igneous provinces: Geology, v. 37, n. 4, p. 323–326, http://dx.doi.org/10.1130/G25325A.1

Ghiorso, M. S., and Sack, R. O., 1995, Chemical mass transfer in magmatic processes IV. A revised and internally consistent thermodynamic model for the interpolation and extrapolation of liquid-solid equilibria in magmatic systems at elevated temperatures and pressures: Contributions to Mineralogy and Petrology, v. 119, n. 2–3, p. 197–212, http://dx.doi.org/10.1007/BF00307281

Green, T. H., and Pearson, N. J., 1987, An experimental study of Nb and Ta partitioning between Ti-rich minerals and silicate liquids at high pressure and temperature: Geochimica et Cosmochimica Acta, v. 51, n. 1, p. 55–62, http://dx.doi.org/10.1016/0016-7037(87)90006-8

Griffin, W. L., Pearson, N. J., Belousova, E., Jackson, S. E., van Achterberg, E., O'Reilly, S. Y., and Shee, S. R., 2000, The Hf isotope composition of cratonic mantle: LAM-MC-ICMPS analysis of zircon megacrysts in kimberlites: Geochimica et Cosmochimica Acta, v. 64, p. 133–147, http://dx.doi.org/10.1016/S0016-7037(99)00343-9

Griffin, W. L., Belousova, E. A., Shee, S. R., Pearson, N. J., and O'Reilly, S. Y., 2004, Archean crustal evolution in the northern Yilgarn Craton: U-Pb and Hf-isotope evidence from detrital zircons: Precambrian Research, v. 131, p. 231–282, http://dx.doi.org/10.1016/j.precamres.2003.12.011

Griffin, W. L., Belousova, E. A., Walters, S. G., and O'Reilly, S. Y., 2006a, Archaean and Proterozoic crustal evolution in the Eastern Succession of the Mt Isa District, Australia: U-Pb and Hf-isotope studies of detrital zircons: Australian Journal of Earth Sciences, v. 53, n. 1, p. 125–150, http://dx.doi.org/10.1080/08120090500434591

Griffin, W. L., Pearson, N. J., Belousova, E. A., and Saeed, A., 2006b, Comment: Hf-isotope heterogeneity in zircon 91500: Chemical Geology, v. 233, n. 3–4, p. 358–363, http://dx.doi.org/10.1016/j.chemgeo.2006.03.007

Harris, N. B. W., and Marriner, G. F., 1980, Geochemistry and petrogenesis of a peralkaline granite complex form the Midian Mountains, Saudi Arabia: Lithos, v. 13, n. 4, p. 325–337, http://dx.doi.org/10.1016/0024-4937(80)90052-3

Hart, S. R., and Dunn, T., 1993 Experimental cpx/melt partitioning of 24 trace elements: Contributions to Mineralogy and Petrology, v. 113, n. 1, p. 1–8, http://dx.doi.org/10.1007/BF00320827

Hauri, E. H., Wagner, T. P., and Grove, T. L., 1994, Experimental and natural partitioning of Th, U, Pb and other trace elements between garnet, clinopyroxene and basaltic melts: Chemical Geology, v. 117, n. 1–4, p. 149–166, http://dx.doi.org/10.1016/0009-2541(94)90126-0

He, B., Xu, Y.-G., Huang, X.-L., Luo, Z.-Y., Shi, Y.-R., Yang, O.-J., and Yu, S.-Y., 2007, Age and duration of the Emeishan flood volcanism, SW China: Geochemistry and SHRIMP zircon U-Pb dating of silicic ignimbrites, post-volcanic Xuanwei Formation and clay tuff at the Chaotian section: Earth and Planetary Science Letters, v. 255, p. 306–323, http://dx.doi.org/10.1016/j.epsl.2006.12.021

Hou, T., Zhang, Z., Kusky, T., Du, Y., Liu, J., and Zhao, Z., 2011, A reappraisal of the high-Ti and low-Ti classification of basalts and petrogenetic linkage between basalts and mafic-ultramafic intrusions in the Emeishan large igneous province, SW China: Ore Geology Reviews, v. 41, n. 1, p. 133–143, http://dx.doi.org/10.1016/j.oregeorev.2011.07.005

Huppert, H. E., and Sparks, R. S. J., 1988, The generation of granitic magmas by intrusion of basalt into continental crust: Journal of Petrology, v. 29, n. 3, p. 599–624, http://dx.doi.org/10.1093/petrology/29.3.599

Irvine, T. N., 1977, Origin of chromitite layers in the Muskox intrusion and other stratiform intrusions: A new interpretation: Geology, v. 5, n. 5, p. 273–277, http://dx.doi.org/10.1130/0091-7613(1977)5⟨273:OOCLIT⟩2.0.CO;2

Jakobsen, J, K., Veksler, I. V., Tegner, C., and Brooks, C. K., 2005, Immiscible iron- and silica-rich melts in basalt petrogenesis documented in the Skaergaard intrusion: Geology, v. 33, n. 11, p. 885–888, http://dx.doi.org/10.1130/G21724.1

Kempton, P. D., Fitton, J. G., Saunders, A. D., Nowell, G. M., Taylor, R. N., Hardarson, B. S., and Pearson, G., 2000, The Iceland plume in space and time: a Sr-Nd-Pb-Hf study of the North Atlantic rifted margin: Earth and Planetary Science Letters, v. 177, n. 3–4, p. 255–271, http://dx.doi.org/10.1016/S0012-821X(00)00047-9

Lee, C. A., 1996, A review of mineralization in the Bushveld Complex and some other layered mafic intrusions, *in* Cawthorn, R. G. editor, Layered Intrusions: Amsterdam, Elsevier, Developments in Petrology, v. 15, p. 103–145, http://dx.doi.org/10.1016/S0167-2894(96)80006-6

Leeman, W. P., and Scheidegger, K. F., 1977, Olivine/liquid distribution coefficients and a test for crystal-liquid equilibrium: Earth and Planetary Science Letters, v. 35, n. 2, p. 247–257, http://dx.doi.org/10.1016/0012-821X(77)90128-5

Liu, D., Jian, P., Kroner, A., and Xu, S., 2006, Dating of prograde metamorphic events deciphered from episodic zircon growth in rocks of the Dabie-Sulu UHP complex, China: Earth and Planetary Science Letters, v. 250, n. 3–4, p. 650–666, http://dx.doi.org/10.1016/j.epsl.2006.07.043

Ludwig, K. R., 2003, A Geochonological toolkit for Microsoft Excel: Berkeley Geochronological Center, Special Publication, No. 4, 70 p.

Mahood, G. A., and Hildreth, E. W., 1983, Large partition coefficients for trace elements in high-silica rhyolites: Geochimica et Cosmochimica Acta, v. 47, n. 1, p. 11–30, http://dx.doi.org/10.1016/0016-7037(83)90087-X

Maier, W. D., Barnes, S. J., and Marsh, J. S., 2003, The concentrations of the noble metals in Southern African flood-type basalts and MORB: implications for petrogenesis and magmatic sulphide exploration: Contributions to Mineralogy and Petrology, v. 146, n. 1, p. 44–61, http://dx.doi.org/10.1007/s00410-003-0480-z

Marks, M., Halama, R., Wenzel, T., and Markl, G., 2004, Trace element variations in clinopyroxene and amphibole from alkaline to peralkaline syenites and granites: implications for mineral-melt trace-element partitioning: Chemical Geology, v. 211, n. 3–4, p. 185–215, http://dx.doi.org/10.1016/j.chemgeo.2004.06.032

Matsui, Y., Onuma, N., Nagasawa, H., Higuchi, H., and Banno, S., 1977, Crystal structure control in trace element partition between crystal and magma: Bulletin de la Société française de Minéralogie et Cristallographie, v. 100, p. 315–324.

McCallum, I. S., 1996, The Stillwater Complex, *in* Cawthorn, R. G. editor, Layered Intrusions: Amsterdam, Elsevier, Developments in Petrology, v. 15, p. 441–483, http://dx.doi.org/10.1016/S0167-2894(96)80015-7

Morse, S. A., 1969, The Kiglapait Layered Intrusion, Labrador: Geological Society of America Memoir 112, 204 p.

——— 1996, Kiglapait mineralogy III: Olivine compositions and Rayleigh fractionation models: Journal of Petrology, v. 37, n. 5, p. 1037–1061, http://dx.doi.org/10.1093/petrology/37.5.1037

Münker, C., Weyer, S., Scherer, E., and Mezger, K., 2001, Separation of high field strength elements (Nb, Ta, Zr, Hf) and Lu from rock samples for MC-ICPMS measurements: Geochemistry Geophysics Geosystems v. 2, n. 12, 1064, http://dx.doi.org/10.1029/2001GC000183

Namur, O., Charlier, B., Toplis, M. J., Higgins, M. D., Hounsell, V., Liégeois, J. P., and Vander Auwera, J., 2011, Differentiation of tholeiitic basalt to A-type granite in the Sept Iles layered intrusion, Canada: Journal of Petrology, v. 52, n. 3, p. 487–539, http://dx.doi.org/10.1093/petrology/egq088

Natali, C., Beccaluva, L., Bianchini, G., and Siena, F., 2011, Rhyolites associated to Ethiopian CFB: Clues for initial rifting at the Afar plume axis: Earth and Planetary Science Letters, v. 312, n. 1–2, p. 59–68, http://dx.doi.org/10.1016/j.epsl.2011.09.059

Nielsen, R. L., 1992, BIGD: A FORTRAN program to calculate trace-element partition coefficients for natural mafic and intermediate composition magmas: Computers and Geosciences, v. 18, n. 7, p. 773–788, http://dx.doi.org/10.1016/0098-3004(92)90024-L

Pang, K.-N., Zhou, M.-F., Lindsley, D., Zhao, D., and Malpas, J., 2008a, Origin of Fe-Ti oxide ores in mafic intrusions: Evidence from the Panzhihua intrusion, SW China: Journal of Petrology, v. 49, n. 2, p. 295–313, http://dx.doi.org/10.1093/petrology/egm082

Pang, K.-N., Li., C., Zhou, M.-F., and Ripley, E. M., 2008b, Abundant Fe-Ti oxide inclusions in olivine from Panzhihua and Hongge layered intrusions, SW China: evidence for early saturation of Fe-Ti oxides in ferrobasaltic magma: Contributions to Mineralogy and Petrology, v. 156, n. 3, p. 307–321, http://dx.doi.org/10.1007/s00410-008-0287-z

——— 2009, Mineral compositional constraints on petrogenesis and oxide ore genesis of the late Permian Panzhihua layered gabbroic intrusion, SW China: Lithos, v. 110, n. 1–4, p. 199–214, http://dx.doi.org/10.1016/j.lithos.2009.01.007

Pang, K.-N., Zhou, M.-F., Qi, L., Shellnutt, J. G., Wang, C. Y., and Zhao, D., 2010, Flood basalt related Fe-Ti-V oxide deposits in the Emeishan large igneous province, SW China: Lithos, v. 119, n. 1–2, p. 123–136, http://dx.doi.org/10.1016/j.lithos.2010.06.003

Potts, P. J., Thompson, M., Kane, J. S., and Petrov, L. L., 2000, GEOPT7—An international proficiency test for analytical geochemistry laboratories: Report on Round 7, 35 p.

Potts, P. J., Thompson, M., Webb, P. C., and Watson, J. S., 2001, GEOPT9—An international proficiency test for analytical geochemistry laboratories: Report on Round 9, 36 p.

Price, J. D., Hogan, J. P., Gilbert, M. C., London, D., and Morgan VI, G. B., 1999, Experimental study of titanite-fluorite equilibria in the A-type Mount Scott granite: Implications for assessing F contents of felsic magma: Geology, v. 27, n. 10, p. 951–954, http://dx.doi.org/10.1130/0091-7613(1999)027⟨0951:ESOTFE⟩2.3.CO;2

Qi, L., and Zhou, M.-F., 2008, Platinum-group elemental and Sr-Nd-Os isotopic geochemistry of Permian Emeishan flood basalts in Guizhou Province, SW China: Chemical Geology, v. 248, n. 1–2, p. 83–103, http://dx.doi.org/10.1016/j.chemgeo.2007.11.004

Qi, L., Jing, H., and Gregoire, D. C., 2000, Determination of trace elements in granites by inductively coupled plasma mass spectrometry: Talanta, v. 51, n. 3, p. 507–513, http://dx.doi.org/10.1016/S0039-9140(99)00318-5

Qi, L., Wang, C. Y., and Zhou, M.-F., 2008 Controls on the PGE distribution of Permian Emeishan alkaline and peralkaline volcanic rocks in Longzhoushan, Sichuan Province, SW China: Lithos, v. 106, n. 3–4, p. 222–236, http://dx.doi.org/10.1016/j.lithos.2008.07.012

Roeder, P. L., and Emslie, R. F., 1970, Olivine Equilibrium: Contributions to Mineralogy and Petrology, v. 29, n. 4, p. 275–289, http://dx.doi.org/10.1007/BF00371276

Rollinson, H. R., 1993, Using Geochemical Data: Evaluation, Presentation, Interpretation: Essex, Longman, 352 p.

Ruddnick, R. L., and Gao, S., 2003, Composition of the continental crust, *in* Rudnick, R. L. editor, The Crust: Treatise on Geochemistry, v. 3, p. 1–64, http://dx.doi.org/10.1016/B0-08-043751-6/03016-4

Sandecki, J., 2000, Mineralogical and genetical aspects of the Smålands Taberg Fe-Ti-V ore, Protogine zone of southern Sweden: GFF, v. 122, n. 4, p. 351–358, http://dx.doi.org/10.1080/11035890001224351

Scherer, E., Münker, C., and Mezger, K., 2001, Calibration of the lutetium-hafnium clock: Science, v. 293, n. 5530, p. 683–687, http://dx.doi.org/10.1126/science.1061372

Schissel, D., and Smail, R., 2001, Deep-mantle plumes and ore deposits: Geological Society of America Special Paper, v. 352, p. 291–322, http://dx.doi.org/10.1130/0-8137-2352-3.291

Shellnutt, J. G., and Iizuka, Y., 2011, Mineralogy from three peralkaline granitic plutons of the Late Permian Emeishan large igneous province (SW China): evidence for contrasting magmatic conditions of A-type granitoids: European Journal of Mineralogy, v. 23, n. 1, p. 45–61, http://dx.doi.org/10.1127/0935-1221/2010/0022-2073

Shellnutt, J. G., and Jahn, B.-M., 2010, Formation of the Late Permian Panzhihua plutonic-hypabyssal-volcanic igneous complex: Implications for the genesis of Fe-Ti oxide deposits and A-type granites of SW China: Earth and Planetary Science Letters, v. 289, n. 3–4, p. 509–519, http://dx.doi.org/10.1016/j.epsl.2009.11.044

——— 2011, Origin of Late Permian Emeishan basaltic rocks from the Panxi region (SW China): Implications for the Ti-classification and spatial-compositional distribution of the Emeishan flood basalts: Journal of Volcanology and Geothermal Research, v. 199, n. 1–2, p. 85–95, http://dx.doi.org/10.1016/j.jvolgeores.2010.10.009

Shellnutt, J. G, and Zhou, M.-F., 2007, Permian peralkaline, peraluminous and metaluminous A-type granites in the Panxi district, SW China: Their relationship to the Emeishan mantle plume: Chemical Geology, v. 243, n. 3–4, p. 286–316, http://dx.doi.org/10.1016/j.chemgeo.2007.05.022

Shellnutt, J. G., Zhou, M.-F., Yan, D. P., and Wang, Y., 2008, Longevity of the Permian Emeishan mantle plume (SW China): 1 Ma, 8 Ma or 18 Ma?: Geological Magazine, v. 145, n. 3, p. 373–388, http://dx.doi.org/10.1017/S0016756808004524

Shellnutt, J. G., Zhou, M.-F., and Zellmer, G., 2009a, The role of Fe-Ti oxide crystallization in the formation of A-type granitoids with implications for the Daly gap: An example from the Permian Baima igneous complex, SW China: Chemical Geology, v. 259, n. 3–4, p. 204–217, http://dx.doi.org/10.1016/j.chemgeo.2008.10.044

Shellnutt, J. G., Wang, C. Y., Zhou, M.-F., and Yang, Y. H., 2009b, Zircon Lu-Hf isotopic compositions of metaluminous and peralkaline A-type granitic plutons of the Emeishan large igneous province (SW China): Constraints on the mantle source: Journal of Asian Earth Sciences, v. 35, n. 1, p. 45–55, http://dx.doi.org/10.1016/j.jseaes.2008.12.003

Shellnutt, J. G., Jahn, B.-M., and Dostal, J., 2010, Elemental and Sr-Nd isotope geochemistry of microgranular enclaves from peralkaline A-type granitic plutons of the Emeishan large igneous province, SW China: Lithos, v. 119, n. 1–2, p. 34–46, http://dx.doi.org/10.1016/j.lithos.2010.07.011

Shellnutt, J. G., Denyszyn, S. W., and Mundil, R., 2011a, Precise age determination of mafic and felsic intrusive rocks from the Permian Emeishan large igneous province (SW China): Gondwana Research, http://dx.doi.org/10.1016/j.gr2011.10.009

Shellnutt, J. G., Jahn, B.-M., and Zhou, M.-F., 2011b, Crustally-derived granites in the Panzhihua region, SW China: Implications for felsic magmatism in the Emeishan large igneous province: Lithos, v. 123, n. 1–4, p. 145–157, http://dx.doi.org/10.1016/j.lithos.2010.10.016

Smith, P. M., and Asimow, P. D., 2005, Adiabat_1ph: a new public front-end to the MELTS, pMELTS, and pHMELTS models: Geochemistry Geophysics Geosytems, v. 6, n. 1, Q02004, http://dx.doi.org/10.1029/2004GC000816

Song, X. Y., Zhou, M.-F., Hou, Z. Q., Cao, Z. M., Wang, Y. L., and Li, Y., 2001, Geochemical constraints on the mantle source of the upper Permian Emeishan continental flood basalts, southwestern China: International Geology Review, v. 43, n. 3, p. 213–225, http://dx.doi.org/10.1080/00206810109465009

Song, X. Y., Zhou, M.-F., Cao, Z. M., and Robinson, P. T., 2004, Late Permian rifting of the South China craton caused by the Emeishan mantle plume?: Journal of the Geological Society, v. 161, p. 773–781, http://dx.doi.org/10.1144/0016-764903-135

Song, X. Y., Qi, H. W., Robinson, P. T., Zhou, M.-F., Cao, Z. M., and Chen, L. M., 2008, Melting of the subcontinental lithospheric mantle by the Emeishan mantle plume; evidence from the basal alkaline basalts in Dongchuan, Yunnan, Southwestern China: Lithos, v. 100, n. 1–4, p. 93–111, http://dx.doi.org/10.1016/j.lithos.2007.06.023

Speczik, S., Wiszniewska, J., and Diedel, R., 1988, Minerals, exsolution features and geochemistry of Fe-Ti ores of the Suwalki district (North-East Poland): Mineralium Deposita, v. 23, n. 3, p. 200–210, http://dx.doi.org/10.1007/BF00204302

Sun, S. S., and McDonough, W. F., 1989, Chemical and isotopic systematics of oceanic basalts: implications for mantle composition and processes, *in* Saunders, A. D., and Norry, M. J., editors, Magmatism in the Ocean Basins: Geological Society, London, Special Publications, v. 42, p. 313–435, doi:10.1144/GSL.SP.1989.042.01.19

Tao, Y., Li, C., Hu, R., Qi, L., Qu, W., and Du, A., 2010, Re-Os isotopic constraints on the genesis of the Limahe Ni-Cu deposit in the Emeishan large igneous province, SW China: Lithos, v. 119, n. 1–2, p. 137–146, http://dx.doi.org/10.1016/j.lithos.2010.02.006

Thompson, M., Potts, P. J., Kane, J. S., and Wilson, S., 1999, GEOPT5—An international proficiency test for analytical geochemistry laboratories: Report on Round 5, 23 p.

Veksler, I. V., Dorfman, A. M., Danyushevsky, L. V., Jakobsen, J. K., and Dingwell, D. B., 2006, Immiscible silicate liquid partition coefficients: implications for crystal-melt element partitioning and basalt Petrogenesis: Contributions to Mineralogy and Petrology, v. 152, n. 6, p. 685–702, http://dx.doi.org/10.1007/s00410-006-0127-y

Veksler, I. V., Dorfman, A. M., and Borisov, A. A., Wirth, R., and Dingwell, D. B., 2007, Liquid Immiscibility and the Evolution of Basaltic Magma: Journal of Petrology, v. 48, n. 11, p. 2187–2210, http://dx.doi.org/10.1093/petrology/egm056

Vervoort, J. D., and Blichert-Toft, J., 1999, Evolution of the depleted mantle: Hf isotope evidence from juvenile rocks through time: Geochimica et Cosmochimica et Acta, v. 63, n. 3–4, p. 533–556, http://dx.doi.org/10.1016/S0016-7037(98)00274-9

Villemant, B., Jaffrezic, H., Joron, J. L., and Treuil, M., 1981, Distribution coefficients of major and trace elements—fractional crystallization in the alkali basalt series of Chaîne-Des-Puys (Massif Central, France): Geochimica et Cosmochimica Acta, v. 45, n. 11, p. 1997–2016, http://dx.doi.org/10.1016/0016-7037(81)90055-7

Wager, L. R., and Brown, G. M., 1968, Layered Igneous Rocks: Edinburgh, Oliver and Boyd, 588 p.

Wang, C. Y., Zhou, M.-F., and Qi, L., 2007, Permian flood basalts and mafic intrusions in the Jinping (SW China)–Song Da (northern Vietnam) district: Mantle sources, crustal contamination and sulfide segregation: Chemical Geology, v. 243, n. 3–4, p. 317–343, http://dx.doi.org/10.1016/j.chemgeo.2007.05.017

Wang, D. R., Xie, Y. M., Hu, Y. J., You, X. X., and Cao, J. X., 1993, Geology of Guogailiang area (Map

G-48-1-A): Panxi Geological Team, Geology and Mineral Resources Bureau, Sichuan Province, scale 1: 50,000.

Weibe, R. A., 1996, Mafic-silicic layered intrusions: the role of basaltic injections on magmatic processes and the evolution of silicic magma chambers: Transactions of the Royal Society of Edinburgh: Earth Sciences, v. 87, p. 233–242, http://dx.doi.org/10.1017/S0263593300006647

White, J. C., Ren, M., and Parker, D. F., 2005, Variation in mineralogy, temperature, and oxygen fugacity in a suite of strongly peralkaline lavas and tuffs, Pantelleria, Italy: The Canadian Mineralogist, v. 43, n. 4, p. 1331–1347, http://dx.doi.org/10.2113/gscanmin.43.4.1331

Wiedenbeck, M., Allé, P., Corfu, F., Griffin, W. L., Meier, M., Oberli, F., von Quadt, A., Roddick, J. C., and Spiegel, W., 1995, Three natural zircon standards for U-Th-Pb, Lu-Hf trace element and REE analyses: Geostandards and Geoanalytical Research, v. 19, n. 1, p. 1–23, http://dx.doi.org/10.1111/j.1751-908X.1995.tb00147.x

Wones, D. R., 1989, Significance of the assemblage titanite + magnetite + quartz in granitic rocks: American Mineralogist, v. 74, p. 744–749.

Woodhead, J. D., and Hergt, J. M., 2005, A preliminary appraisal of seven natural zircon reference materials for *in situ* Hf isotope determination: Geostandards and Geoanalytical Research, v. 29, n. 2, p. 183–195, http://dx.doi.org/10.1111/j.1751-908X.2005.tb00891.x

Xiao, L., Xu, Y.-G., Chung, S.-L., He, B., and Mei, H., 2003 Chemostratigraphic correlation of Upper Permian lavas from Yunnan Province, China: Extent of the Emeishan large igneous province: International Geology Review, v. 45, n. 8, p. 753–766, http://dx.doi.org/10.2747/0020-6814.45.8.753

Xiao, L., Xu, Y.-G., Mei, H. J., Zheng, Y. F., He, B., and Pirajno, F., 2004, Distinct mantle sources of low-Ti and high-Ti basalts from the western Emeishan large igneous province, SW China: implications for plume-lithosphere interaction: Earth and Planetary Science Letters, v. 228, n. 3–4, p. 525–546, http://dx.doi.org/10.1016/j.epsl.2004.10.002

Xu, Y., Chung, S.-L., Jahn, B.-M., and Wu, G., 2001, Petrologic and geochemical constraints on the petrogenesis of Permian-Triassic Emeishan flood basalts in southwestern China: Lithos, v. 58, n. 3–4, p. 145–168, http://dx.doi.org/10.1016/S0024-4937(01)00055-X

Xu, Y.-G., He, B., Chung, S.-L., Menzies, M. A., and Frey, F. A., 2004 Geologic, geochemical, and geophysical consequences of plume involvement in the Emeishan flood-basalt province: Geology, v. 32, n. 10, p. 917–920, http://dx.doi.org/10.1130/G20602.1

Xu, Y.-G., Luo, Z. Y., Huang, X. L., He, B., Xiao, L., Xie, L. W., and Shi, Y. R., 2008, Zircon U-Pb and Hf isotope constraints on crustal melting associated with the Emeishan mantle plume: Geochimica et Cosmochimica Acta, v. 72, n. 1, p. 3084–3104, http://dx.doi.org/10.1016/j.gca.2008.04.019

Yao, P. H., Wang, K. N., Du, C. L., Lin, Z. T., and Song, X., 1993, Records of China's Iron Ore Deposits: Beijing, Metallurgic Industry Press, p. 633–649 (in Chinese with English abstract).

Zhang, Z., Mao, J., Saunders, A. D., Ai, Y., Li, Y., and Zhao, L., 2009, Petrogenetic modeling of three mafic-ultramafic layered intrusions in the Emeishan large igneous province, SW China, based on isotopic and bulk chemical constraints: Lithos, v. 113, n. 3–4, p. 369–392, http://dx.doi.org/10.1016/j.lithos.2009.04.023

Zhong, H., Zhou, X. H., Zhou, M.-F., Sun, M., and Liu, B. G., 2002, Platinum-group element geochemistry of the Hongge Fe-V-Ti deposit in the Pan-Xi area, southwestern China: Mineralium Deposita, v. 37, n. 2, p. 226–239, http://dx.doi.org/10.1007/s00126-001-0220-0

Zhong, H., Yao, Y., Prevec, S. A., Wilson, A. H., Viljoen, M. J., Viljoen, R. P., Liu, B. G., and Luo, Y. N., 2004, Trace-element and Sr-Nd isotopic geochemistry of the PGE-bearing Xinjie layered intrusion in SW China: Chemical Geology, v. 203, n. 3–4, p. 237–252, http://dx.doi.org/10.1016/j.chemgeo.2003.10.008

Zhong, H., Campbell, I. H., Zhu, W. G., Allen, C. M., Hu, R. Z., Xie, L. W., and He, D. F., 2011, Timing and source constraints on the relationship between mafic and felsic intrusions in the Emeishan large igneous province: Geochimica et Cosmochimica Acta, v. 75, n. 5, p. 1374–1395, http://dx.doi.org/10.1016/j.gca.2010.12.016

Zhou, M.-F., Malpas, J., Song, X. Y., Robinson, P. T., Sun, M., Kennedy, A. K., Lesher, C. M., and Keays, R. R., 2002, A temporal link between the Emeishan large igneous province (SW China) and the end-Guadalupian mass extinction: Earth and Planetary Science Letters, v. 196, n. 3–4, p. 113–122, http://dx.doi.org/10.1016/S0012-821X(01)00608-2

Zhou, M.-F., Robinson, P. T., Lesher, C. M., Keays, R. R., Zhang, C. J., and Malpas, J., 2005, Geochemistry, petrogenesis and metallogenesis of the Panzhihua gabbroic layered intrusion and associated Fe-Ti-V oxide deposits, Sichuan Province, SW China: Journal of Petrology, v. 46, n. 11, p. 2253–2280, http://dx.doi.org/10.1093/petrology/egi054

Zhou, M.-F., Arndt, N. T., Malpas, J., Wang, C. Y., and Kennedy. A. K., 2008, Two magma series and associated ore deposit types in the Permian Emeishan large igneous province, SW China: Lithos, v. 103, n. 3–4, p. 352–368, http://dx.doi.org/10.1016/j.lithos.2007.10.006